Testing of the SPEDE conversion electron spectrometer at ISOLDE

Pro Gradu, 10.04.2017

Author:

Joonas Ojala

Supervisor:

Janne Pakarinen

CERN-THESIS-2017-264
//2017

JYVÄSKYLÄN YLIOPISTO
FYSIIKAN LAITOS

Tiivistelmä

Joonas Ojala
SPEDE-ilmaisimen testaus ISOLDE-laboratoriossa
Pro Gradu-tutkielma
Fysiikan laitos, Jyväskylän yliopisto, 2017, 45 sivua.

Työssä testattiin uutta SPEDE-ilmaisinta CERNin ISOLDE-laboratorion MINIBALL-koeasemalla, jossa selvitetään ytimien rakenteita käyttämällä radioaktiivia suihkuja. Ilmaisimen testauksessa käytettiin radioaktiivisia Bi-207 ja Hg-191 lähteitä. SPEDE-ilmaisimella pystytään havaitsemaan sisäisen konversion elektroneja. Ytimen viritystilan purkautumisessa sisäinen konversio on kilpaileva prosessi tavanomaisemmalle γ-emissiolle. Sisäistä konversiota tutkimalla saadaan selvitettyä ytimen rakenteen ominaisuuksia kuten esimerkiksi E0-siirtymät ytimissä. SPEDE-ilmaisin mahdollistaa samanaikaiset γ- ja elektronispektrometriset mittaukset MINIBALL-koeasemalla. Työssä käytettiin kokeellisten mittaustulosten tukena GEANT4-simulaatio-ohjelmalla saatuja tuloksia. Työn tuloksina saatiin määritettyä $\alpha_{K/L}$-kerroin Bi-207 konversioelektroneille, siirtymälle $5/2^- \rightarrow 1/2^-$ $\alpha_{K/L} = 3.29 \pm 0.06$ ja siirtymälle $13/2^+ \rightarrow 5/2^-$ $\alpha_{K/L} = 3.11 \pm 0.05$. Lisäksi työssä määritettiin osittainen konversiokerroin Au-191 siirtymälle $5/2^+ \rightarrow 3/2^+$ $\alpha_{Kmeas} = 0.30 \pm 0.13$, jolle on määritetty teoreettinen arvo $\alpha_{Ktheor} = 0.28 \pm 0.01$. Testin tuloksena voidaan todeta, että SPEDE kykenee toimimaan tulevissa mittauksissa MINIBALL-koeasemalla mahdollistaen uuden tavan tutkia ytimien rakenteita. Osa tuloksista ei ollut yhtenäisiä vanhoihin tuloksiin tai teoreettisiin laskelmiin. Tämän selittää käytetty elektroniikka, mikä ei ollut täysin yhteensopiva SPEDEn kanssa.

Avainsanat: Sisäinen konversio, elektronispektrometri, SPEDE, ISOLDE, MINIBALL

Abstract

Joonas Ojala
Testing of the SPEDE conversion electron spectrometer at the ISOLDE
Master's thesis
Department of Physics, University of Jyväskylä, 2017, 45 pages.

The aim of this work was to test the performance of the SPEDE detector in the MINIBALL setup at CERN's ISOLDE laboratory. The main research objective of MINIBALL is to study properties of atomic nuclei employing radioactive ion beams. Radioactive Bi-207 and Hg-191 were used in this experiment. SPEDE detects internal conversion electrons which are created in transitions between states in atomic nucleus. The internal conversion is competing process to more common γ-ray emission. This way it is possible to measure different properties of nuclear structure for example the E0-transitions. The simultaneous γ and electron measurements are possible when SPEDE is used in conjunction with the MINIBALL spectrometer. The GEANT4 simulation results were used to help interpretation of experimental results. As a result, $\alpha_{K/L}$-ratio was determined for Bi-207 conversion electrons, for the $5/2^- \rightarrow 1/2^-$ transition $\alpha_{K/L} = 3.29 \pm 0.06$ and for the $13/2^+ \rightarrow 5/2^-$ transition $\alpha_{K/L} = 3.11 \pm 0.05$ were obtained. Also, the partial internal conversion coefficient $\alpha_{Kmeas} = 0.30 \pm 0.13$ was determined for Au-191 for the $5/2^+ \rightarrow 3/2^+$ transition , which is well in-line with the theoretical value $\alpha_{Ktheor} = 0.28 \pm 0.01$. Some of the results are inconsistent with theory and previous results, which can be explained by the electronics used in tests. One can still say that SPEDE is capable to measure in future experiments in MINIBALL-experimental setup. SPEDE will bring new possibility to explore nuclear structure in MINIBALL.

Keywords: Internal conversion, electron spectrometer, SPEDE, ISOLDE, MINIBALL

Preface

The experimental part of this work has been done in ISOLDE laboratory at CERN during summer 2016. It was done during my research training for Helsinki Institute of Physics (HIP). The summer 2016 was filled with work and education. On the other hand, it was also enjoyable and fun at the same time.

I would like to thank my supervisor Dr. Janne Pakarinen for choosing me to this work and for guidance and answering my questions about physics and problems which was encountered during writing of this thesis. I have learned a lot about detectors, particle detection and physics. In addition, I want to express my gratitude for Dr. Daniel Cox for his guidance and help with measurements and my problems with ROOT and GEANT4.

I also want to thank Mr. Topi Löytäinen for reading this thesis through. I also want to thank all colleagues and FYS4 community from department. Without your support this work could not be done.

Kiitokset myös äiteelle, isseelle sekä siskolleni tuesta opiskeluvuosina. Ilman teidän opetuksia ja neuvoja, en olisi päässyt tänne asti. Kiitoksen myös ansaitsevat ystävät ja kaverit, jotka antoivat minulle muuta ajateltavaa fysiikan ulkopuolelta.

Jyväskylä, 2017

Joonas Ojala

Contents

1 Introduction

The structure of matter has fascinated even ancient civilizations. One of the earliest theory of matter was proposed by Empedocles (ca. 490-430 B.C.E.) who claimed that all matter consist of four indestructible elements–fire, water, air and earth [1]. Democritus (ca. 460-370 B.C.E.) took the next step by proposing that all matter is composed of atoms and an atom is indivisible [2]. He also claimed that atoms could posses' different shapes and sizes. However, these antique theories of matter are more close to philosophy than empirical science. Next leap was the first observation of atom made by John Dalton (1766-1844) [3]. Hundred year later, the nucleus was discovered by Rutherford (1871-1937) in his famous gold foil experiment [4]. Nowadays it is known that nucleus consists of protons and neutrons, while proton and neutron consists of quarks. The structure of nucleus holds still many secrets; spectrometers can be used to reveal these mysteries.

SPectrometer for Electron DEtection (SPEDE) is silicon detector that is used to detect electrons from internal conversion. Internal conversion is process which competes with γ-ray emission to de-excite excited states in atomic nucleus. SPEDE will be used in conjunction with the MINIBALL spectrometer at Isotope Separator On Line DEvice (ISOLDE). Measuring simultaneously internal conversion electrons and γ-rays provides information on the structure of nuclei that can not be obtained when measuring either γ-rays or conversion electrons alone. SPEDE will be used in Coulomb excitation experiments employing Radioactive Ion Beams(RIB)s from the HIE-ISOLDE post-accelerator. In this thesis experiment, radioactive sources were used.

ISOLDE is located at CERN, the European Organization for Nuclear Research. ISOLDE employs protons from Proton-Synchrotron Booster (PSB) which is preaccelator for the famous Large Hadron Collider (LHC). MINIBALL is one of many experimental setups at ISOLDE. ISOLDE has diverse physics programme, but large proportion of studies are focused to exotic nuclei and nuclear structure.

This thesis is divided into five topics; theoretical framework, experimental aspects, simulations, analysis, and conclusions. Theoretical framework deal with basic concepts of nuclear physics–shell model, internal conversion, Coulomb excitation, etc., which are key concepts in future experiments with SPEDE. Experimental aspects section covers main concepts of detecting electrons and γ-rays, describes ISOLDE and the MINIBALL setup, the SPEDE spectrometer and description of this experiment. Simulation includes basics of GEANT4 and the SPEDE-experimental setup simulations. The analysis section explains methods used in this thesis and results. Conclusions are given in the last section.

2 Theoretical framework

2.1 Principals of nuclear properties

Nucleus consists of A nucleons; Z protons and N neutrons. In addition to mass, important properties of nucleus are binding energy, angular momentum, half-life, radius and energy levels. These properties depend on nucleus internal structure; how nucleons are organized in states and how nucleons form the nucleus.

The nucleus itself is quantum mechanical object and inside nucleus there are three interacting forces which "glue" nucleons together; Coulomb force, strong interaction and weak interaction. The Coulomb force is repulsive interaction between protons which can be described as a force between two charged particles

$$F = \frac{1}{4\pi\varepsilon_0}\frac{q_1 q_2}{r^2}, \tag{1}$$

where q_1 and q_2 are charges of particles and r the distance between these particles. Strong interaction is a short-range force which keeps neighbouring nucleons together. The effect of weak interaction is seen in β decays and electron capture (EC) process.

Interacting forces generate potential for individual nucleon inside nucleus. This potential can be described using the so-called Wood-Saxon potential and can be parametrized as

$$U(r) = \frac{-U_0}{1 + \exp(r - R_0)/a}, \tag{2}$$

where $U(r)$ is potential energy as a function of radius of nucleus with following parameters; R_0, U_0, and a. R_0 is usually determined following way $R_0 = r_0 A^{\frac{1}{3}}$ where r_0 is usually between 1.25-1.27. Typical values for $U_0 \approx 50$MeV and $a \approx 0.6$fm [5, 6].

2.2 Shell model

The shell model, introduced by Ivanenko et al. [7], proposed that nucleus has similar structure as electron shell structure of atom. Shell structure can be experimentally observed e.g. from neutron (S_n, S_{2n}) and proton (S_p, S_{2p}) separation energies. The separation energy has the local maximum at certain proton or neutron numbers, often referred as magic numbers (2, 8, 20, 28, 50, 82, 126) that represents the major shells of nuclei. If one treats each nucleon individually in its potential created by other nucleons, nucleons occupy also subshells inside major shell [2]. Subshells can be seen in figure 1.

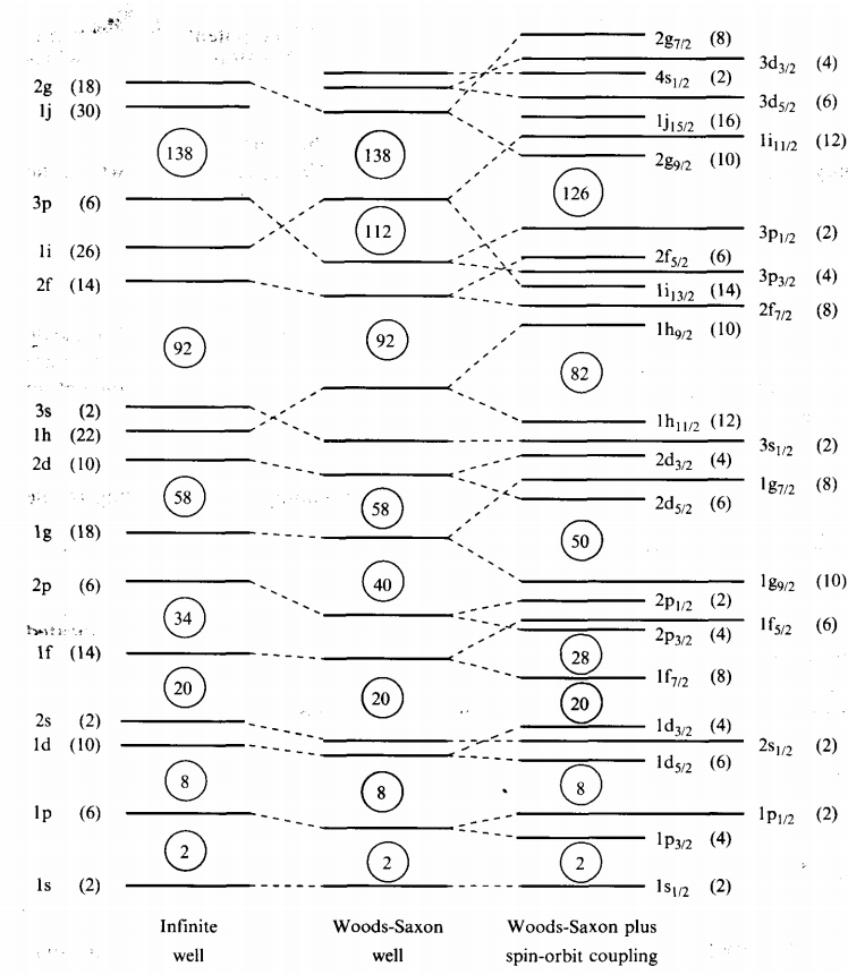

Figure 1: Single-particle states calculated with different nuclear potentials. Figure taken from [5].

These major shells and subshells were explained by Mayer, Haxel, Suess and Jensen. The nuclear potential was known to look like as Wood-Saxon potential (equation (2)) but it did not explain these major shells. Mayer et al. added the spin-orbit term to Wood-Saxon potential which described these major shells

$$V_{so}(r)\,\langle l \cdot s\rangle = V_{so}\frac{1}{2}[j(j+1) - l(l+1) - s(s+1)]\hbar^2, \tag{3}$$

where $V_{so}(r)$ describe strength of the potential, j is total angular momentum, l orbital angular momentum and s is the spin of the single nucleon [5]. The effect of spin-orbit term can be seen in figure 1. These shells describe the energy levels what nucleons can occupy.

This shell model depends only radius (r) so the potential is central. Central potential is limited only to describe properties of spherical nuclei [8]. To describe potential of deformed nuclei, one needs also take in to take also account polar and azimuthal angles of the spherical coordinates (θ, ϕ) [8].

2.3 Electromagnetic transitions in nuclei

The intrinsic structure and excited states in nucleus can be explored by measuring γ-rays and internal conversion electrons which are emitted in the decay of excited states. Electromagnetic transition in nucleus occurs between initial (angular momentum J_i) and final (angular momentum J_f). This transition creates a γ-ray (known as a γ photon), internal conversion electron or electron-positron pair via internal pair formation. In figure 2, decay scheme of Bi-207 and electromagnetic transitions of excited states in Pb-207 are shown. The transition energy corresponds to the energy difference between the involved initial and final states. Internal conversion will be discussed later on in more details.

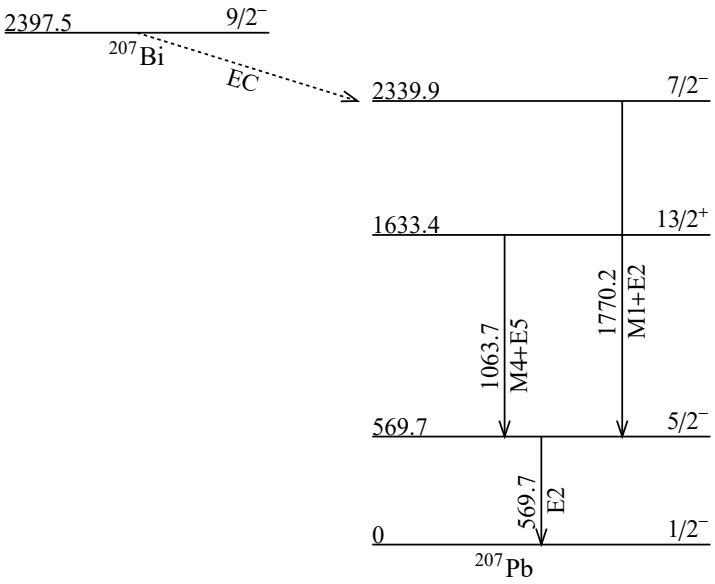

Figure 2: Partial decay scheme of Bi-207.

The electromagnetic transition can be described by multipolarity λ and by field type Θ. The different multipolarities describe different types of transitions, monopole transition ($\lambda = 0$), dipole transition ($\lambda = 1$), quadrupole transition ($\lambda = 2$), octupole transition ($\lambda = 3$). The field types are electric (E) or magnetic (M). The multipolarity λ is restricted by the selection rule

$$|J_i - J_f| \leq \lambda \leq J_i + J_f \tag{4}$$

and $\lambda = 0$ is forbidden transition multipolarity for γ-ray decays. However, an E0 transition is possible via internal conversion electrons and pair creation process [6]. Pure transitions are transitions that have no mixing of other multipolarities due to the selection rule. For example, a $2_1 \rightarrow 0_0$ transition is a pure E2 transition, while a $0^+ \rightarrow 0^+$ transition can only proceed via an E0 transition. The electromagnetic transition obeys parity conservation rules

$$\pi_i \pi_f = \begin{cases} (-1)^{\lambda} & \text{for E}\lambda, \\ (-1)^{\lambda-1} & \text{for M}\lambda, \end{cases} \tag{5}$$

where π_i and π_f are parities of initial and final state, respectively.

The probability of transition between initial state $|\xi_i, J_i\rangle$ and final state $|\xi_f, J_f\rangle$ can be calculated as follows

$$P_{fi}^{(\sigma\lambda)} = \frac{2}{\varepsilon_0 \hbar} \frac{\lambda + 1}{\lambda \left[(2\lambda + 1)!!\right]^2} \left(\frac{E_\gamma}{\hbar c}\right)^{2\lambda+1} B\left(\sigma\lambda; \xi_i J_i \rightarrow \xi_f J_f\right), \tag{6}$$

where σ represents all the other quantum numbers except total angular momentum [8]. Reduced transition probability can be written as [8]

$$B\left(\sigma\lambda;\xi_i J_i \rightarrow \xi_f J_f\right) = \frac{1}{2J_i+1}\left|\left(\xi_f J_f \left|\left|M_{\sigma\lambda}\right|\right| \xi_i J_i\right)\right|^2. \tag{7}$$

Transition probability usually decrease with increasing multipolarity. However, in some cases the E2 transition can be more probable than the M1 transition [8]. For example, Pt-191 has many transitions where the E2 transition is more probable than the M1 transition [9]. In this work, transitions following the decay of Bi-207 and Hg-191 radioactive sources were measured with SPEDE and cluster detectors of MINIBALL.

2.4 Deformed nuclei

An atomic nucleus is not always spherical, but can be deformed in shape. Deformed nucleus cannot be described by using the spherical shell model. The surface of the deformed nucleus can be declared by using radius vector [6]

$$R\left(\theta,\phi\right) = R_0\left(1+\sum_{\lambda\mu}\alpha_{\lambda\mu}Y_{\lambda\mu}\left(\theta,\phi\right)\right), \tag{8}$$

where R_0 is radius of spherical nucleus of same volume and λ is the multipolarity. Assuming axially symmetric deformation leads to $\mu = 0$ (note that for $\alpha_{\lambda 0}$ notation β_λ is used) [6]. Quadrupole deformation ($\lambda = 2$) is often of interest in nuclear physics experiments. In those cases, equation (8) can also be expressed as

$$R\left(\theta,\phi\right) = R_0\left(1+\beta_2 Y_{20}\left(\theta,\phi\right)\right), \tag{9}$$

where β_2 is known as deformation parameter. The deformation parameter β_2 gives information about eccentricity of the ellipse shape nucleus

$$\beta_2 = \frac{4}{3}\sqrt{\frac{\pi}{5}}\frac{\Delta R}{R_0}, \tag{10}$$

where ΔR is the difference between of semimajor and semiminor axis length [2]. By definition, the shape of nuclei is

- spherical, when $\beta_2 = 0$,
- oblate, when $\beta_2 < 0$,
- prolate, when $\beta_2 > 0$.

The deformation parameter β_2 can be acquired by measuring quadrupole moments. Quadrupole moments can be measured in Coulomb excitation experiments. More detailed information on quadrupole moments can be found in [6, 10, 11, 12]. The structure of nucleus can be assessed by measuring the electric monopole E0 strengths [13, 14, 15]. The internal conversion electrons can be detected with SPEDE, which allows for measuring the E0-transitions at the MINIBALL experimental setup.

2.5 Radioactive decays

Most of the known nuclei are unstable. The decay type depends on the neutron-proton ratio and the mass of the nucleus. Common decay modes are $\beta^{\pm}$ and α decays but nuclei can decay through proton-, neutron- or even heavy ion (fission)-decay [5]. There is other process for β^{+} decay known as EC, where proton captures an electron from the atomic orbit and transform to a neutron and a neutrino.

The radioactive-decay law can be written is as follows

$$A = -\frac{dN(t)}{dt}, \tag{11}$$

where A is activity, $N(t)$ is the number of decays and t is time. The $N(t)$ is described by exponential function

$$N(t) = N_0 \cdot e^{-\lambda \cdot t}, \tag{12}$$

where N_0 is the number of nuclei at $t = 0$ and λ is the decay constant. The relation between decay constant and half-life is

$$t_{\frac{1}{2}} = \frac{ln2}{\lambda}, \tag{13}$$

Half-life is time elapsed for the half of sample to decay.

Q-value describes the energy release of radioactive decay. The Q-value is defined as [5]

$$Q = (m_i - m_f)c^2, \tag{14}$$

where m_i is initial mass and m_f is mass of decay products. Radioactive decay is possible if reaction's Q-value is positive. Otherwise, external energy is needed for reaction to take place.

In decay process, the transforming nuclei are called as a parent nucleus and its product as a child nucleus. The radioactive decay can feed the excited states in the child nucleus. These excited states usually decay to the ground state via γ-ray or conversion electron emission.

2.6 Internal conversion

As mentioned in section 2.3, electromagnetic transition can occur via internal conversion. In internal conversion, the excitation energy is transmitted through Coulomb interaction to atomic electron. It should be noted, that internal conversion is not a two-step process, where γ-ray would transfer the energy to atomic electron. The internal conversion is competing process for γ-ray decay. The kinetic energy of electron can be calculated as

$$K_e = \Delta E_{exc} - B_l, \tag{15}$$

where B_l is the binding energy of electron and ΔE_{exc} is the energy difference between initial and final state. The nuclear recoil energy is neglected in equation (15). The binding energy of electron depends on the electron shell. The kinetic energy of conversion

electron can be measured by using spectrometers like SPEDE. The K-shell electron has usually the largest probability to be ejected in internal conversion, on the other hand the L-shell electron can be usually found in spectrum. Difference between internal conversion and β-decay spectrum is that the spectrum of β-decay is continuous rather than discrete peaks as in spectrum of conversion electrons.

Typical quantities of interest for internal conversion are internal conversion coefficient (ICC) α and ratio of emitted K-shell and L-shell electrons ($\alpha_{K/L}$-ratio). These values are used in this work to determine capability of the simultaneous γ-electron measurements of SPEDE. ICC is defined as follows

$$\alpha = \frac{\lambda_e}{\lambda_\gamma} = \alpha_K + \alpha_L + \ldots, \tag{16}$$

where α is the total ICC for corresponding transition, λ_e and λ_γ is decay constant for electron and γ-ray and α_K,$\alpha_L, \ldots$ are partial ICC to each atomic shell [2]. The partial ICC α_K is defined as

$$\alpha_K = \frac{N_{eK}}{N_\gamma}, \tag{17}$$

where N_{eK} is number of emitted electrons from atomic shell K and N_γ number of emitted γ-rays. The partial ICC for L-shell, M-shell, ... is defined similarly. Measurements of ICCs are important for acquiring knowledge of total transition rates. The ICC values depend on the following properties [13]

- ICC values decrease by increasing transition energy
- Values increase by increasing value of multipolarity λ
- Values increase by increasing value of atomic number Z
- Electron shell and its binding energy B
- Nuclear structure.

Theoretical calculations for ICCs are discussed in references [16, 17]. An on-line tool called BrICC is available for ICC calculations at [18].

One of the commonly used conversion ratio is $\alpha_{K/L}$-ratio

$$\alpha_{K/L} = \frac{\alpha_K}{\alpha_L}. \tag{18}$$

The ratio depends strongly on transition multipolarity which makes it useful tool to determine multipolarity [13].

An E0-transition can be happened via internal conversion but not through γ decay. The E0-transition can only happen when initial and final state have the same angular momentum and parity. Of particular interest are the E0-transitions between the $0^+ \rightarrow 0^+$ states, because they carry out information on nuclear radii and possible deformations [6]. The $0^+ \rightarrow 0^+$ transition can only happen via E0-transition due to selection rule (4). Measuring the $0^+ \rightarrow 0^+$ transitions is one of the reasons to equip the MINIBALL spectrometer with SPEDE.

2.7 Coulomb excitation

The inelastic Coulomb scattering, where projectile exchange energy with target, is known as Coulomb excitation [2]. Assumption in Coulomb excitation is that the interaction between positively charged particles, projectile and target nuclei, is purely electromagnetic [19]. Thus, projectile and target keep their identity but target or projectile (or both) nuclei are excited.

Coulomb excitation was introduced in the 1950s. Using Coulomb excitation, it is possible to measure electromagnetic matrix elements. Therefore, the Coulomb excitation experiments allow for nuclear structure information to be inferred.

Multiple-step Coulomb excitation requires more energy than single-step. In low-energy Coulomb excitation (also known as "safe" Couloumb excitation), the distance in head-on collision must be greater than

$$d > [1.25(A_P^{\frac{1}{3}} + A_T^{\frac{1}{3}}) + 5]\text{fm}), \tag{19}$$

where d is distance, A_P is projectile's mass number and A_T is target's mass number [19]. The distance d is needed to assure that interaction between projectile and target is purely electromagnetic [19, 20].

In future SPEDE will be used in Coulomb excitation experiments. SPEDE will increase possibilities to measure nuclear structure at the MINIBALL experimental setup. With SPEDE, E0-transitions can be measured via multistep Coulomb excitation. The advent of the HIE-ISOLDE post-accelerator will allow for beam energies that are needed to enhance the amount of multistep excitations [21].

3 Experimental aspects

3.1 Spectroscopy based on semiconductors

In γ-ray and electron spectroscopy, semiconductor materials are commonly used as detector material. Germanium is commonly used for the γ-ray spectroscopy, while silicon is often chosen for electron spectroscopy [22]. Excellent energy resolution, compact size and fast timing are the characteristic properties of semiconductor detectors.

γ-rays interact with semiconductor material via photoelectric effect, Compton scattering or pair production [13]. Electrons interact with semiconductor materials via scattering with the atomic electrons, inelastic scattering from nuclei, Rutherford scattering and bremsstrahlung [13]. The amount of electrons (and thus the signal amplitude) is proportional to the energy deposited by incoming γ-ray or particle.

Basically, semiconductor detectors are reversed biased diodes. Detectors need proper conditions (low temperature, high voltage, purified from impurities) to perform. Detection efficiency depends on size of the depletion region and the detector material. To increase size of the depletion region, one should decrease amount charge carriers in semiconductor material [23]. Thickness of the depletion region can be formulated by following equation

$$d = \frac{2V\varepsilon}{eN}^{\frac{1}{2}}, \tag{20}$$

where ε is dielectric constant, V is reverse bias voltage, e electronic charge and N number of impurities in semiconductor material [23]. The noise level of signal can be decreased by lowering temperature of the semiconductor. Lowering temperature decreases the amount of the charge carriers which are created by thermal excitation. The optimal operating temperature depends on material. For example, germanium detectors operating temperature is 77K while for silicon that is 250K.

The signal is produced in semiconductor by interaction of γ-ray or particle. The interacting particle creates an electron-hole cascade in the depletion region. Electrons and holes (i.e. charge carriers) drift in opposite directions in the depletion region. These electrons and holes form a signal in the semiconductor detector. This signal has to be further amplified before being digitised. The height of signal is proportional to the energy deposited. The first amplification is done in preamplifiers which output is a tail pulse as shown figure 3.

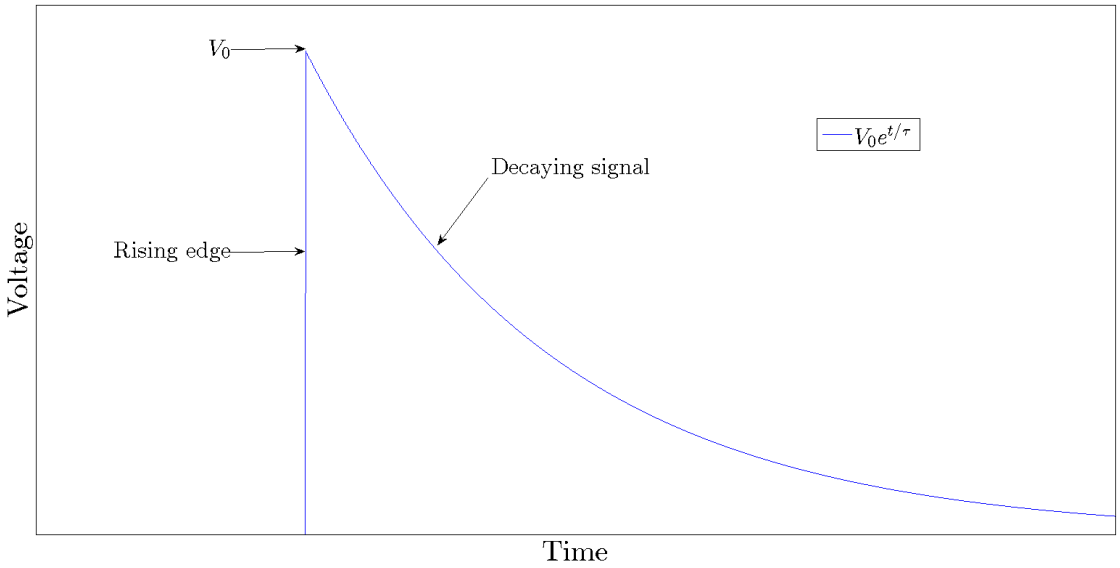

Figure 3: An ideal preamplifier signal. V_0 is amplitude, t is time and τ is the decay-time constant.

One important property of a preamplifier is the decay-time constant τ which describe how fast the preamplified pulse returns back to baseline as seen in figure 3. This information is fed as one parameter into digital data acquisition system.

3.2 The ISOLDE facility

ISOLDE, established in 1967, is one of the laboratories of CERN. The research at ISOLDE is mainly focused in nuclear physics experiments with RIBs. [24]. RIBs give possibility to study different nuclides which are unapproachable or difficult to produce with commonly used stable beams. The layout of ISOLDE can be seen in figure 4.

The radioactive isotopes are produced by impinging 1.4GeV protons from Proton Synchrotron Booster on thick stationary target. The target material depends on desired radioactive isotope; for example, uranium carbide is commonly used. Radioactive atoms are produced via nuclear reactions such as fission and spallation. After collision, radioactive atoms diffuse into ion source. Ion source ionize atoms to 1^+ charge state in hot plasma, on a hot surface or by laser excitation [24]. The ions are accelerated typically to 60keV before mass separation in General Purpose Separator (GPS) or High-Resolution Separator (HRS). The GPS has only one bending magnet but it can distribute beam simultaneously to three different experiment. The HRS consist of two bending magnets and ion-optical system to produce higher mass resolving power.

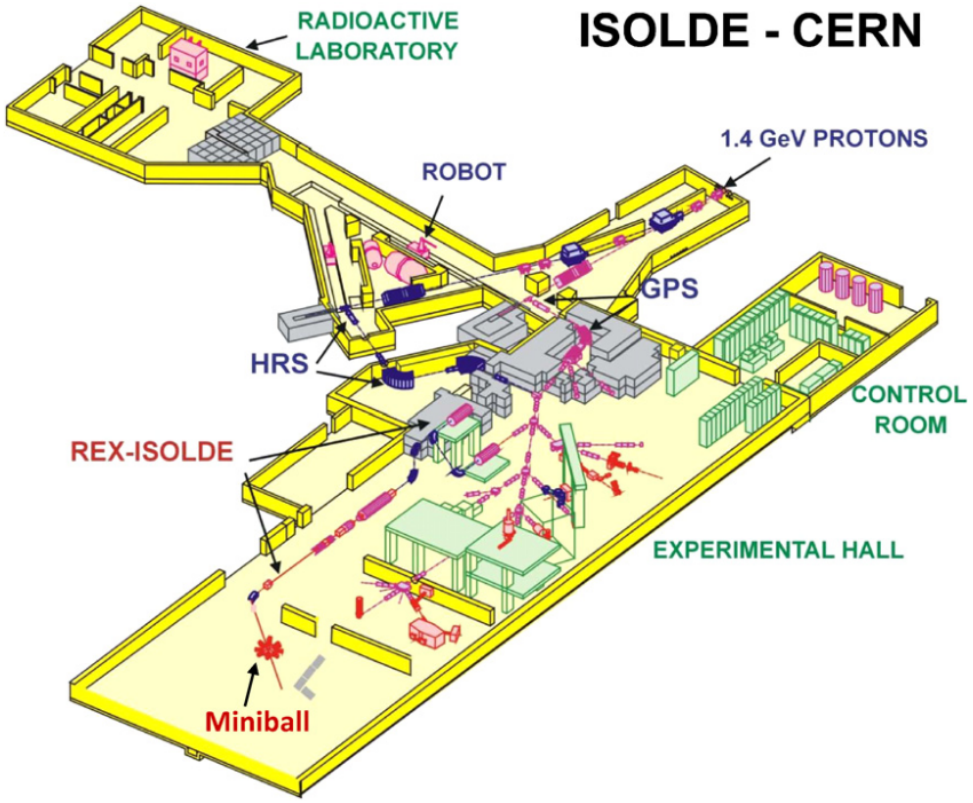

Figure 4: The layout of the ISOLDE laboratory. Figure is taken from [25].

The separated beam, with 1^+ charge state, can be delivered to different experimental setups (see figure 4). Before beam reaches the MINIBALL experiment, it is post-accelerated with HIE-ISOLDE. The HIE-ISOLDE will accelerate RIBs from 60keV up to 10MeV/u [26]. First the RIBs will be cooled and accumulate in Penning trap. The bunch of ions from Penning trap will be charge bred to an optimum charge state in an electron beam ion source and injected to the super conducting linear accelerator HIE-ISOLDE. The HIE-ISOLDE delivers RIBs to the MINIBALL experimental setup [27]. The HIE-ISOLDE is an upgrade of previous post-accelerator REX-ISOLDE.

3.3 The MINIBALL spectrometer

The MINIBALL germanium detector array is one of the ISOLDE experimental setups. The MINIBALL spectrometer consist of 8 cluster detectors and each detector has three germanium crystals. Crystal shape is quasi-cylindrical and is segmented into six equal size piece [28], see schematic figure 7. Crystals are located in the cryostat and are cooled with liquid nitrogen. Detector positions in the frame can be changed which makes it very flexible to different measurements [29]. The MINIBALL spectrometer can be seen in figure 5.

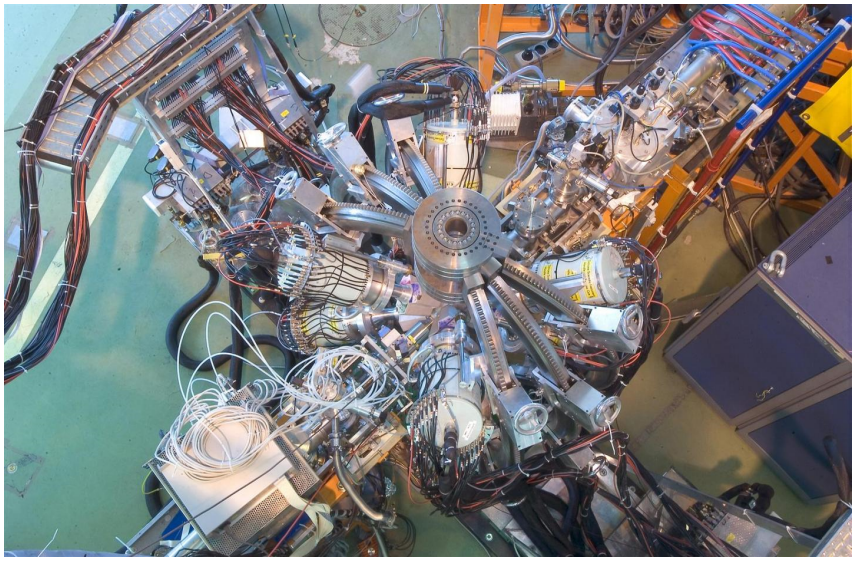

Figure 5: The MINIBALL spectrometer as seen from above. Picture taken from [30].

Each crystal provides seven signals; six signals from outer parts of segments and one signal from core of segments. Therefore, the core signal correspond to the energy sum deposited in the whole crystal. Consequently, each detector delivers 21 signals to be read out by XIA-DGF-4C. Preamplifiers are installed inside the detector. Part of the preamplifiers are in the "warm part" and the other part is in "cold part" of detector as one can see in figure 6. Preamplifiers create heat in "cold part" and are constantly cooled down with liquid nitrogen.

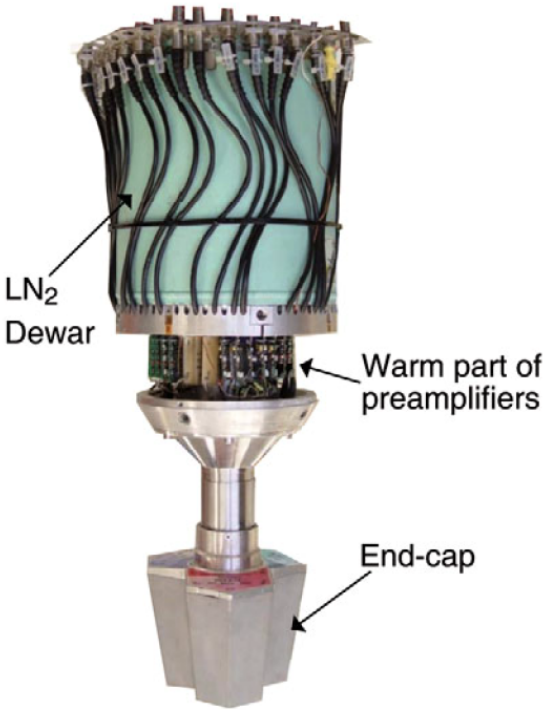

Figure 6: Picture of a MINIBALL triple-cluster germanium detector. The preamplifier housing has been removed for visualisation purposes. Picture taken from [28].

Besides measuring the energy of γ-ray, it is also possible to determine position of the interacting point from crystals segmentation and pulse-shape analysis [29, 28]. The pulse-shape analysis is done on the XIA-DGF-4C board [28].

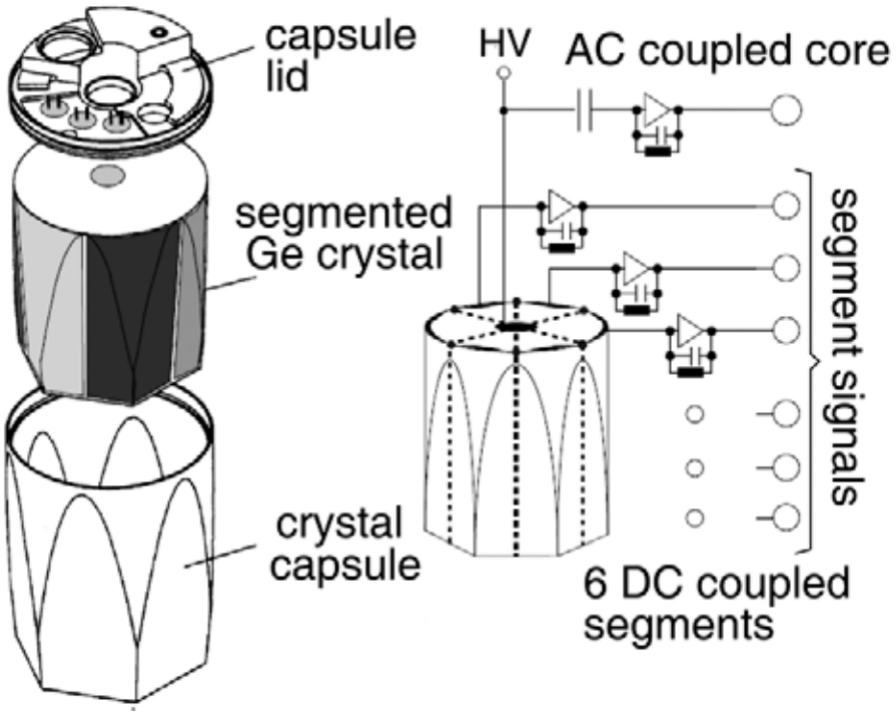

Figure 7: Schematic view of germanium crystal and its segmentation. Figure taken from [28].

MINIBALL can be used in various configurations. For example, MINIBALL has been most commonly used in Coulomb excitation and transfer reaction studies, each having a dedicated target chamber. The SPEDE spectrometer will be an important ancillary device and will be mounted in its own target chamber.

SPEDE will benefit from working in conjunction with MINIBALL. Simultaneous γ-electron measurements allow for coincidence measurements and it is essential for measuring internal conversion coefficients. In addition, γ-electron measurements improve measurements for nucleus's states and decay scheme, especially for low energy transition in heavy nuclei [22].

In this work, two MINIBALL triple-cluster detectors were used at MINIBALL. The experimental setup can be seen in figure 8. One detector was mounted in downstream and another one in upstream from the target. MINIBALL detectors were used to measure γ-rays from radioactive source. This gives possibility to measure coincidences with SPEDE. Two germanium detectors were sufficient for testing the performance of the SPEDE spectrometer with sources.

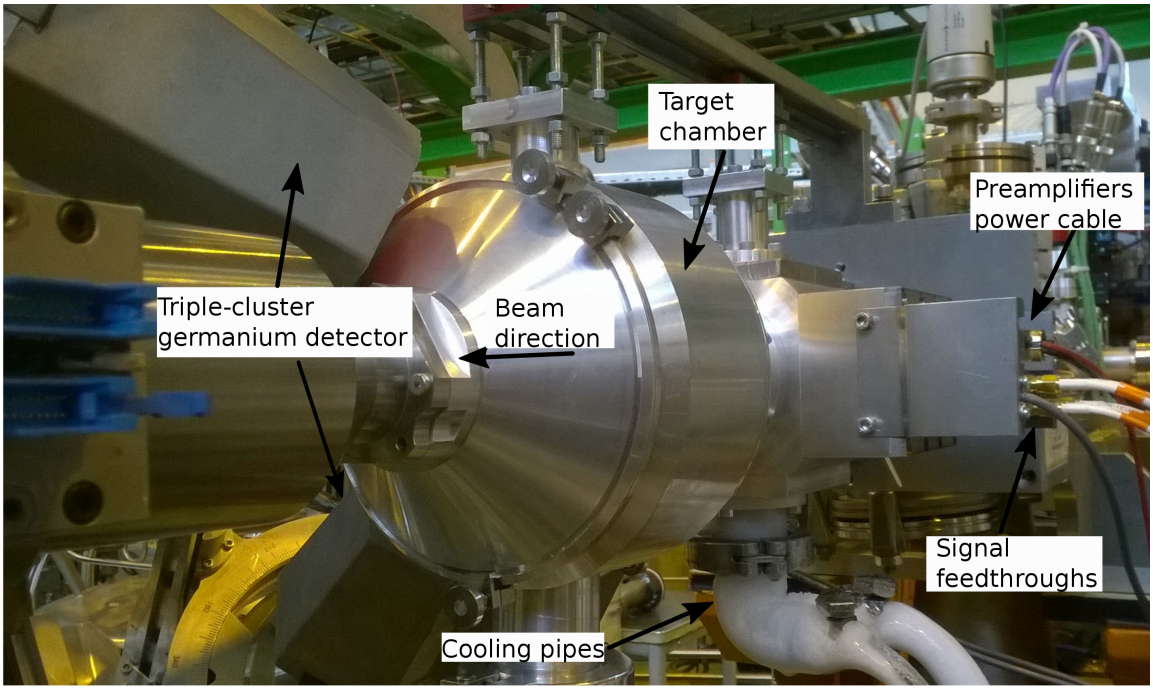

Figure 8: The experimental setup used in this thesis. Essential parts have been labelled.

3.4 The SPEDE spectrometer

SPEDE is a new in-beam electron spectrometer which will be used at ISOLDE. Detector purpose is to measure internal conversion electrons. Both the target nuclei and the detector is inside of target chamber which is specially made for the SPEDE detector. Radioactive beam passes SPEDE through a hole in the centre of the detector before impinging on the target. The target chamber is installed in the centre of the MINIBALL setup. The CD detector (see figure 9) is mounted downstream of target, while the SPEDE detector is installed upstream of the target in the SPEDE target chamber. CD is used to measure energy and hit position of particles.

The SPEDE detector is annularly segmented silicon detector with thickness of 500 µm and positioned at ($\sim$ 2cm) upstream from target [32]. Targets are mounted to a ladder which is mounted in the feedthrough in the bottom of the target chamber. The detector is divided in to 24 equal volume segments to keep capacitance of segments equal [32]. GEANT4 simulations were used to decide number of segments [33]. Segmentation of detector can be seen in figure 10b and more schematic figure 10a.

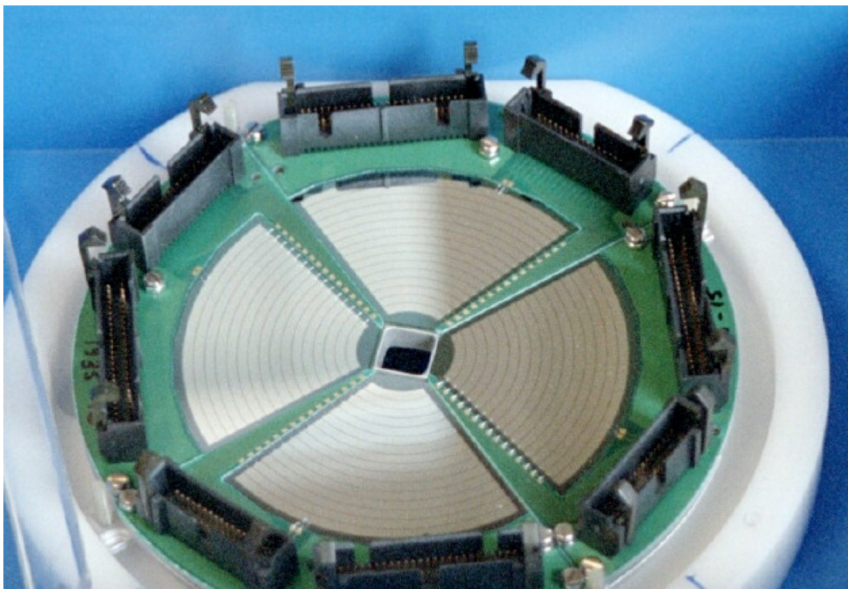

Figure 9: Front-side of the CD detector. Figure taken from [31].

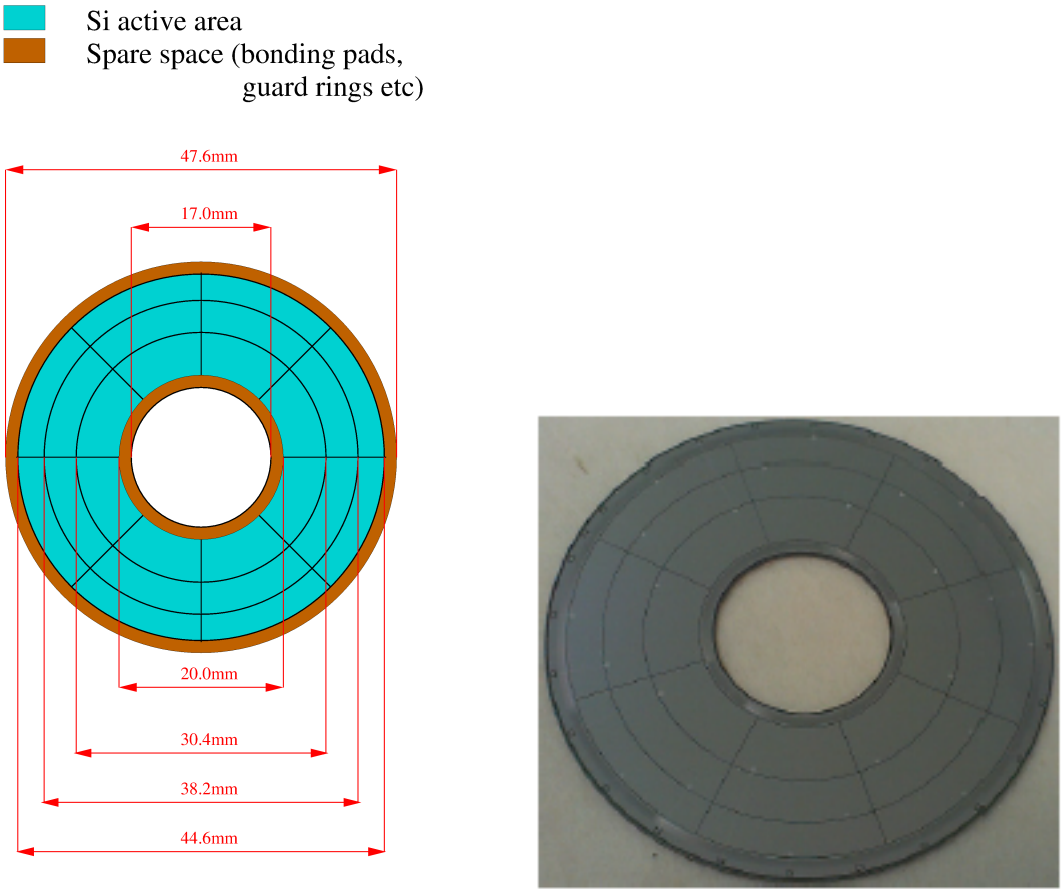

(a) (b)

Figure 10: (a)Schematic figure of the SPEDE dimensions. (b) Photograph of the segmented SPEDE silicon. Picture is taken from [33].

The SPEDE detector is clued on the PCB while the preamplifiers are mounted on its backside [32]. The PCB is chilled with ethanol coolant, which is cooled down by the Julabo cooling unit. The temperature of detector is measured with a PT100 sensor that is mounted on the PCB. Ethanol cooling allows to reach operating temperature of SPEDE silicon at $\sim -10\,^{\circ}\mathrm{C}$ and dissipates the power introduced by preamplifiers. This is essential as the preamplifiers are in vacuum where radiative cooling is not sufficient. SPEDE is biased up to +90V voltage by the Mesytec MHV-4 voltage supply.

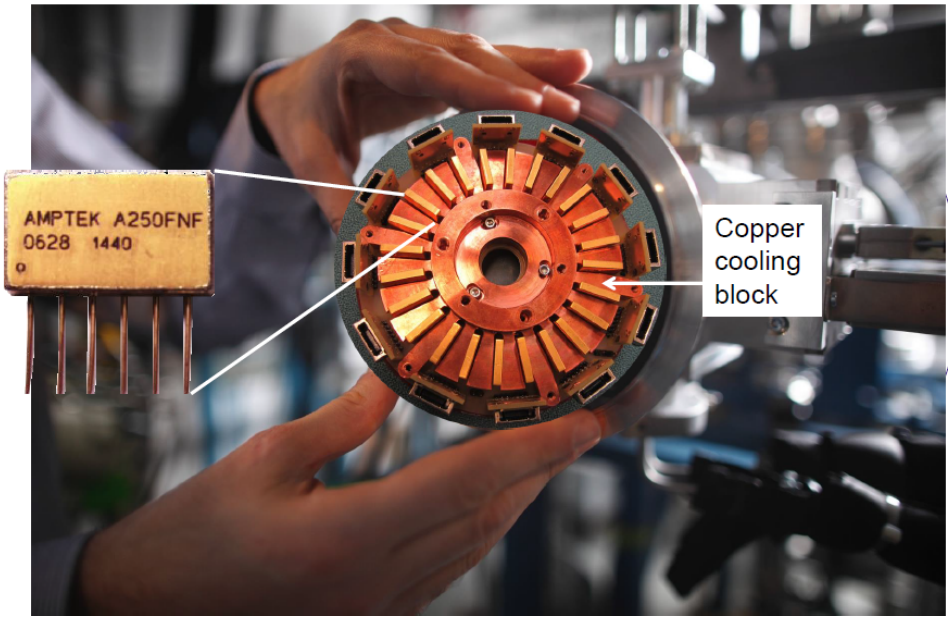

Figure 11: The backside of SPEDE. Preamplifiers and cooling block are labelled. Picture is taken from [34].

Each SPEDE channel is equipped with an Amptek A250F/NF preamplifier, which provides a gain of 0.64uV/electron corresponding to 175mV/MeV [35]. Preamplifiers are powered by Mesytec MNV-4. Signals can be further amplified in the Gain and Offset (GO) unit, which also allows for adjusting the signal offset to match with the input range of the analogue-to-digital converter. In this work 50Ω resistor and 1.2 gain was used in GO-unit. Signals from the GO-unit are fed into the same signal read out system (XIA-DGF-4C) as the germanium detector signals.

In this work, SPEDE performance was tested with Bi-207 and Hg-191 sources. The Hg-191 source was specially made for this measurement. The experimental setup can be seen in figure 8. Since SPEDE was not used in-beam, there was no need to mount the CD detector for these tests (see figure 12). Experimental results are discussed in section 5.

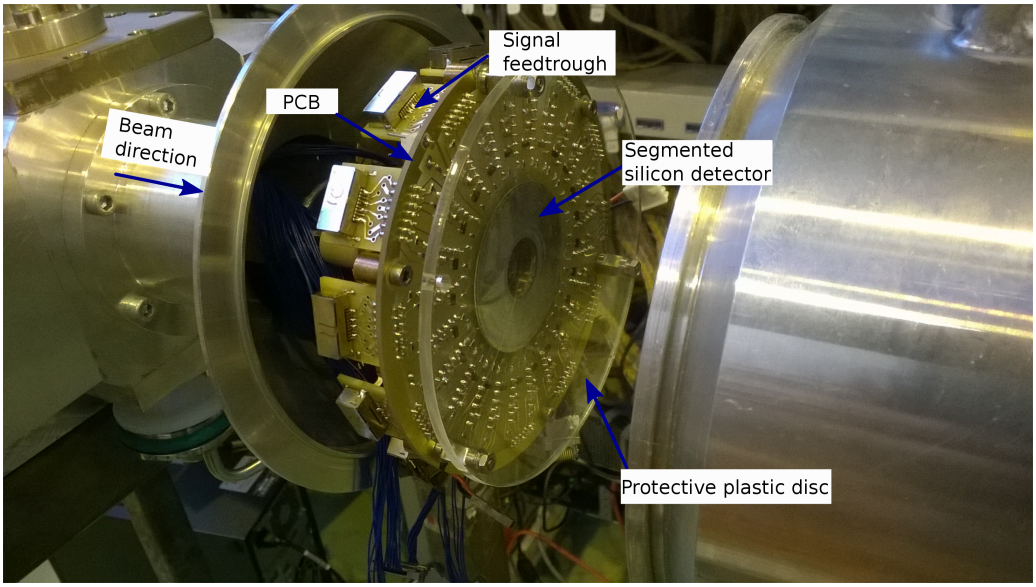

Figure 12: SPEDE installed in the target chamber. Protective plastic disc allowing for easier handling can be seen in in front of SPEDE.

The ion beam ionizes the atoms in the target. In beam-target collisions, so-called delta-electrons and x-rays are created [13, 23]. Flux of the delta-electrons is focused in the direction of the ion beam.

To decrease amount of delta-electrons, SPEDE is installed to upstream from target [33]. This geometry decreases delta-electrons effect in the spectrum and also reduces kinematic broadening. Conversion electron spectrometers often use magnetic and electric fields to transport conversion electrons to reduces the background originating e.g. from delta-electrons and other charged particles. SPEDE does not need electron transportation because the SPEDE detector can be mounted close to the target due to lower intensity of the radioactive ion beam. Low intensity means also lower number of delta-electrons [32]. The delta-electron flux can be further suppressed by applying target in positive high voltage (+5kV) and placing an absorber foil in front of the detector [32].

3.5 The SPEDE signal shape

The SPEDE preamplifier signal has a fast rise time of 4.5ns [35]. The decay of the signal can be divided in to two components with different decay-time constants, $\tau = 10.0\mu$s and $\tau = 100.6\mu$s as shown in figure 13. This resulted in the DGF-4C read-out system having read-out problems and compromised the energy resolution of SPEDE.

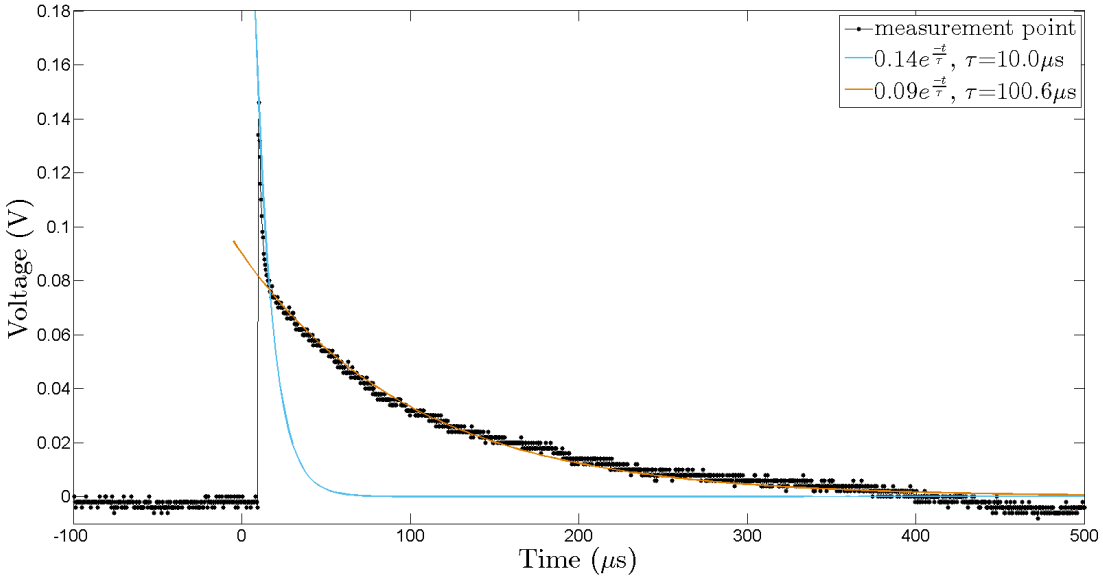

Figure 13: Signal from SPEDE after GO-unit which is read-out by DGF-4C. Signal from SPEDE after GO-unit which is read-out by DGF-4C. The two different fits to the decay are shown with blue and red lines.

The different decay-time constant values between $\tau = 10 - 110\mu$s were tested but even the best acquired resolution was still worse than measured with different digitiser. The signals were tested with Lyrtech cards which gave much better resolution ($\sim 8 - 9$keV). This implies that problem lies in DGF-4C data read-out system. It might be so that DGF-4C is not compatible for signal with two decay-time constants.

3.6 Experimental setup

The purpose of this experiment was to determine the performance of SPEDE combined to the MINIBALL electronics and data acquisition system. The SPEDE spectrometer was mounted in the MINIBALL beam line as in future Coulomb excitation experiments. The vacuum was holding ($\sim 10^{-6}$bar) during testing, which was sufficient for this experiment. The vacuum was pumped in downstream and upstream so that pressure gradient in the target position was minimised. Julabo was set to $\sim -34\,^{\circ}$C degree. A typical SPEDE preamplifier signal can be seen in figure 14.

Two cluster detectors of MINIBALL were used in this experiment. The MINIBALL cluster detectors were cooled with liquid nitrogen autofill system.

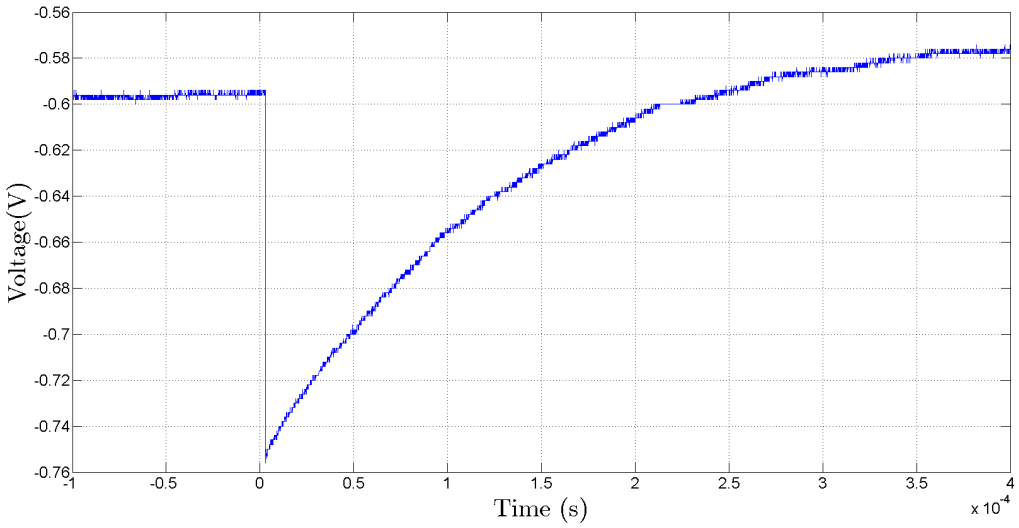

Figure 14: A typical SPEDE preamplifier signal.

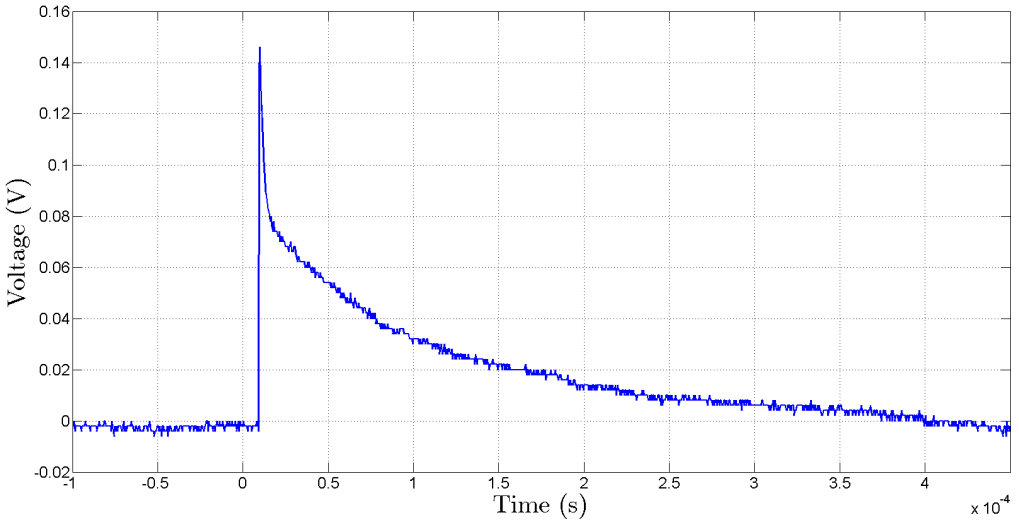

Figure 15: A typical SPEDE signal after the GO-unit with 50Ω resistor and 1.2 gain output settings.

Different electronic configurations and DGF parameters were tested with Bi-207 and Ba-133 sources to improve the resolution. For the GO-unit, 50Ω resistor and 1.2 gain output seemed to be the best option. The GO-unit output can be seen in figure 15. The reason for low resolution is discussed in chapter 5.1.

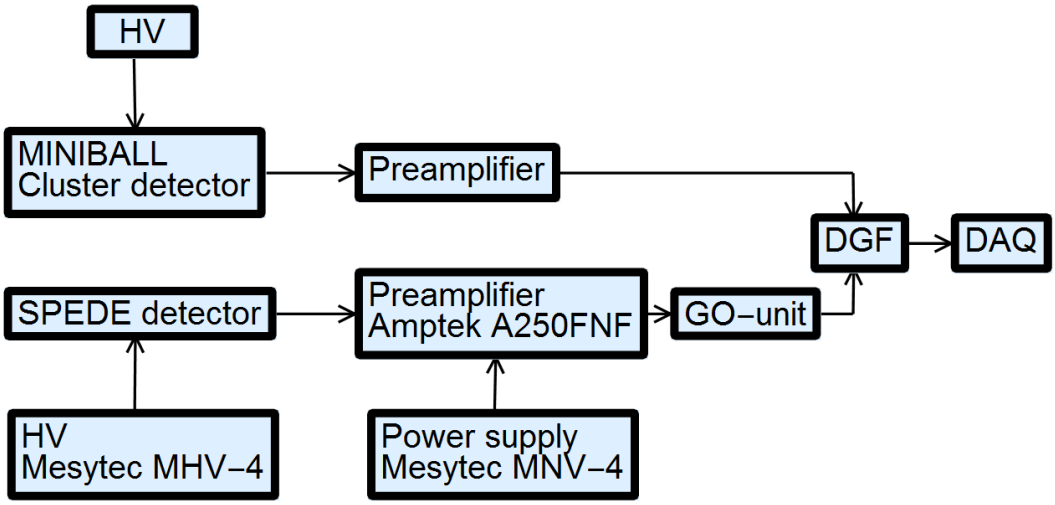

Figure 16: Block diagram showing the fundamental parts of electronics of SPEDE and cluster detector.

The final test setup included SPEDE and two MINIBALL cluster detectors allowing for simultaneous γ-ray and electron detection. Signal from the SPEDE preamplifiers were passed through the GO-unit (50Ω resistor and 1.2 gain-output) and from GO-unit to DGFs. Cluster detector signals were sent directly to DGFs. The block diagram of the MINIBALL+SPEDE-setup is shown in figure 16.

The main objective of testing SPEDE with a Bi-207 source was to extract the $\alpha_{K/L}$ ratio for the $5/2^- \rightarrow 1/2^-$ transition in Bi-207. γ-ray and conversion electron energies and intensities, following the decay of Bi-207, are listed in table 1.

Table 1: Literature values for γ-ray and internal conversion electron energies and intensities following the decay of Bi-207 [36].

Transition	E_γ (keV)	$I_\gamma \pm \Delta_I$ (%)	E_e (keV)	Shell	$I_e \pm \Delta_I$ (%)
$5/2^- \rightarrow 1/2^-$	569.702	97.75±0.39	481.697	K	1.562±0.03
			554.4	L	0.469±0.011
$13/2^+ \rightarrow 5/2^-$	1063.662	74.09±0.24	975.657	K	7.17±0.17
			1048.1	L	1.912±0.055
$7/2^- \rightarrow 5/2^-$	1770.237	6.868±0.028	1682.232	K	0.0237±0.0015
			1754.4	L	0.0038±0.0004

In order to further test the SPEDE performance, a Hg-191 source was prepared using ISOLDE. The Hg-191 decays as follows

$$^{191}\mathrm{Hg} \xrightarrow{EC} {}^{191}\mathrm{Au} \xrightarrow{EC} {}^{191}\mathrm{Pt} \xrightarrow{EC} {}^{191}\mathrm{Ir}, \tag{21}$$

where half-lives for Hg-191 are $t_{1/2} = 49 \pm 10$m and $t_{1/2} = 50.8 \pm 1.5$m, Au-191 is $t_{1/2} = 3.18 \pm 0.08$h, Pt-191 is $t_{1/2} = 2.83 \pm 0.02$d and Ir-191 is stable nucleus [9].

The data-acquisition-system Marabou read data from DGF-4C and produced the ROOT data files. From ROOT-data files, one can create various histograms, detector hitmaps and coincidence matrices for analysis. ROOT is a modular scientific software framework [37] and has been used for analysis in the present work.

4 Simulations

4.1 The GEANT4-simulation toolkit

GEANT4 is object-oriented simulation toolkit for simulating particle interactions with matter. GEANT4 is based on C++ programming language [38] and is developed at CERN. Simulation softwares are essential in modern days physics for better understanding of experimental setups and to help estimate experimental results.

GEANT4 as a Monte Carlo-simulation software toolkit has many functionalities; tracking, geometry, physics models and hits [38]. GEANT4 can handle different materials (silicon, germanium, etc.), elements and particles (electrons, γ-rays, etc.) with energy ranging from 250eV to a TeV. One can build own detector geometries for detectors and visualize particle trajectories. It is also possible to include external electromagnetic fields in simulations. GEANT4 contains also Graphical User Interface (GUI) for visualisation purposes. GEANT4 has been used in different applications in medical, nuclear and radiation physics and space engineering.

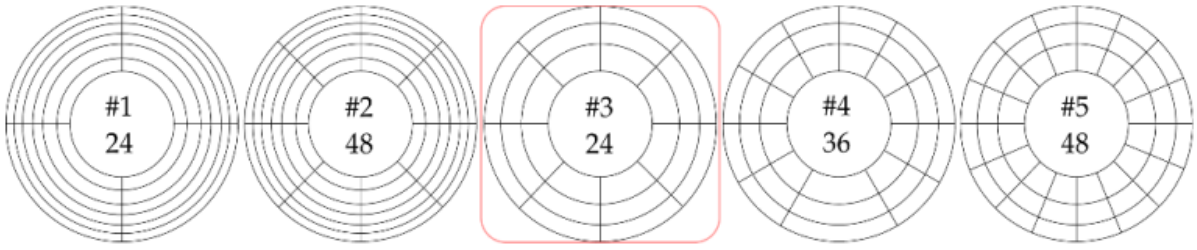

Figure 17: Different silicon detector designs for SPEDE. Figure taken from [33].

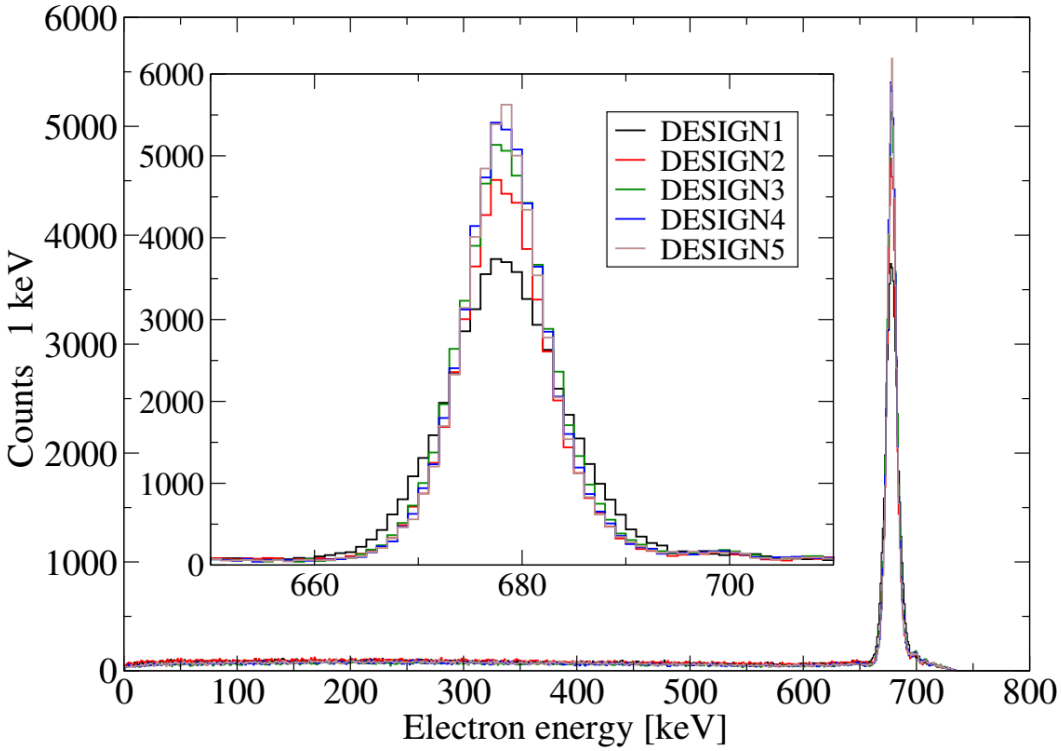

Figure 18: Simulated Coulomb excitation experiment Pb-188 as a beam and Cd-112 as a target. The peak is from recoil gated and kinematically corrected electrons of K-conversion of the 767keV E0-transition in Pb-188. Figure taken from [33].

The SPEDE detector segmentation is based on the GEANT4 simulations (see figure 17 and 18). In simulation, ^{188}Pb was used as a beam and ^{112}Cd as a target. Design 3 was found to meet the required conditions the best [33].

4.2 Simulation of the MINIBALL+SPEDE setup

In this work, GEANT4 was applied to simulate the detection efficiency of SPEDE and MINIBALL. Along the SPEDE detector, the SPEDE simulation includes also the SPEDE target chamber, CD detector and the full MINIBALL array.

The simulation was modified to correspond measurements; the two MINIBALL cluster-detectors were included instead of full array and no CD-detector was mounted in the target chamber. The simulation setup can be seen in figure 19. A flat distribution of pure electron and γ-ray source from 0keV to 3000keV was used in simulation.

The simulation package creates a ROOT file that was used in the analysis. In figure 20 and figure 21, simulated efficiencies for SPEDE and MINIBALL, respectively, are shown.

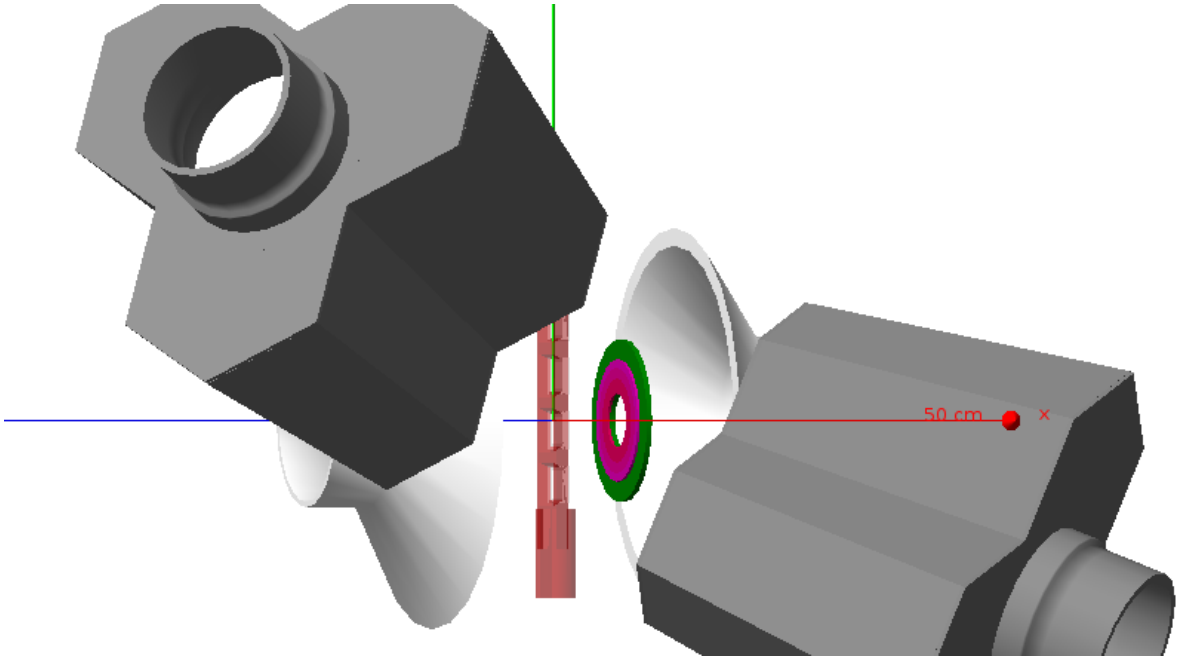

Figure 19: The SPEDE simulation setup; the SPEDE detector and two MINIBALL cluster-detectors. Part of the target chamber was removed for visualisation purposes.

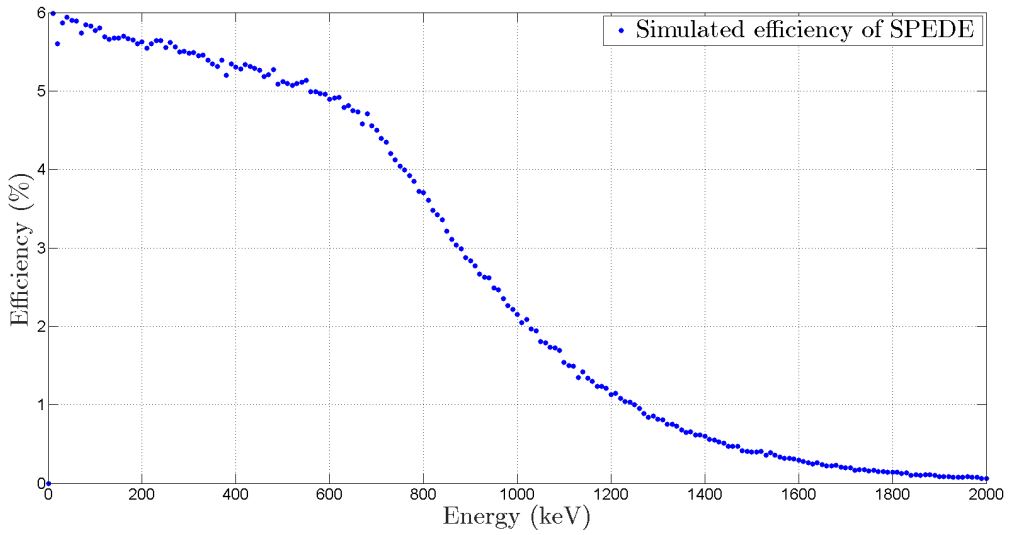

Figure 20: Simulated efficiency of SPEDE by using a flat distribution of electrons.

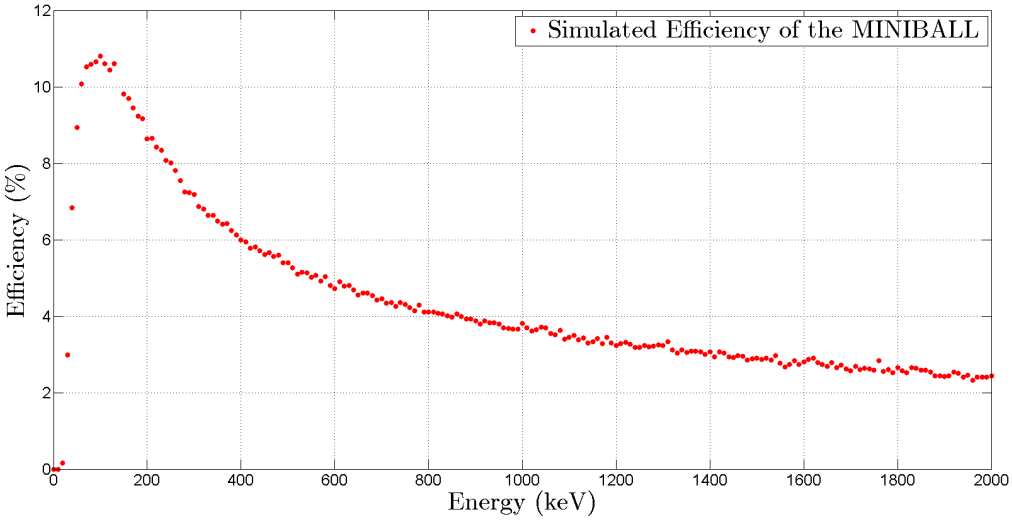

Figure 21: Simulated efficiency of MINIBALL by using a flat distribution of γ-rays.

Ideal conditions of simulations typically result in overestimation of detection efficiency. In real measurements, electronics, cables and many other reasons reduces the total efficiency. However, simulations provide important tool for better understanding of experimental setups. For example, one can see (in figure 20) efficiency rapidly dropping above 600keV energy, which can be explained by electrons passing through the detector and thus depositing only fraction of their kinetic energy. The uncertainty for simulated efficiency was estimated to be 5% of efficiency.

5 Analysis and results

5.1 Experimental results

For Bi-207 and Hg-191, the calibrated electron and γ-ray energy spectra were generated. The FWHM (full width at half-maximum) is one of the parameters which is used to describe the detector performance. The FWHM was measured to be $\sim$ 15keV at 482keV and $\sim$ 19keV at 975keV in Bi-207 measurement. This is clearly worse than what was measured with SPEDE connected to other electronics, e.g. Lyrtech digitiser cards.

The experimental results are visualised in energy spectra shown in figures 22, 23, 24 and 25. The electron energy spectra show the total singles measured with SPEDE, ie. where all pixels are summed together. The γ-ray energy spectra have been formed similar way by summing the energy spectra from cores of the segments.

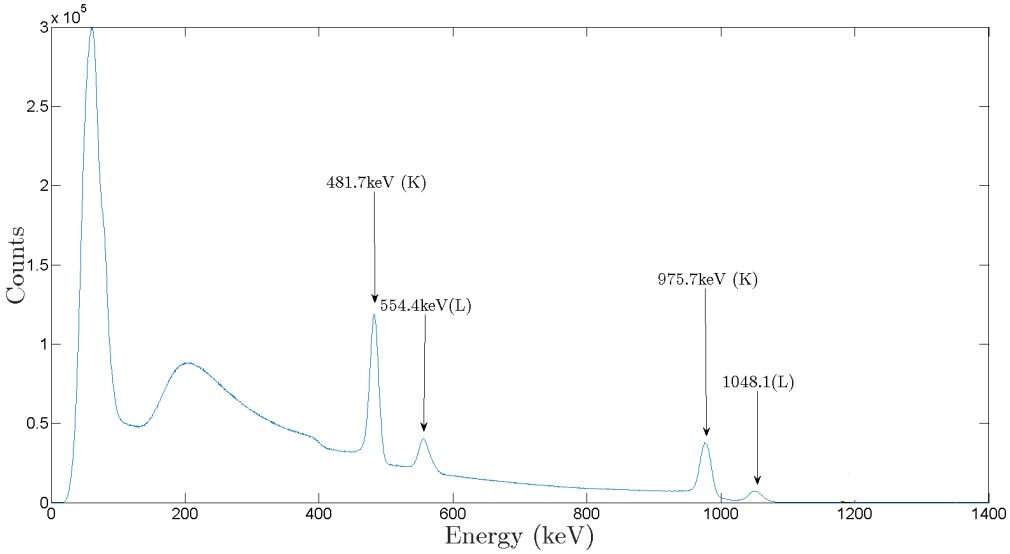

Figure 22: Bi-207 electron energy spectrum measured with SPEDE. The most prominent peaks have been labelled according to electron energy and corresponding atomic shell.

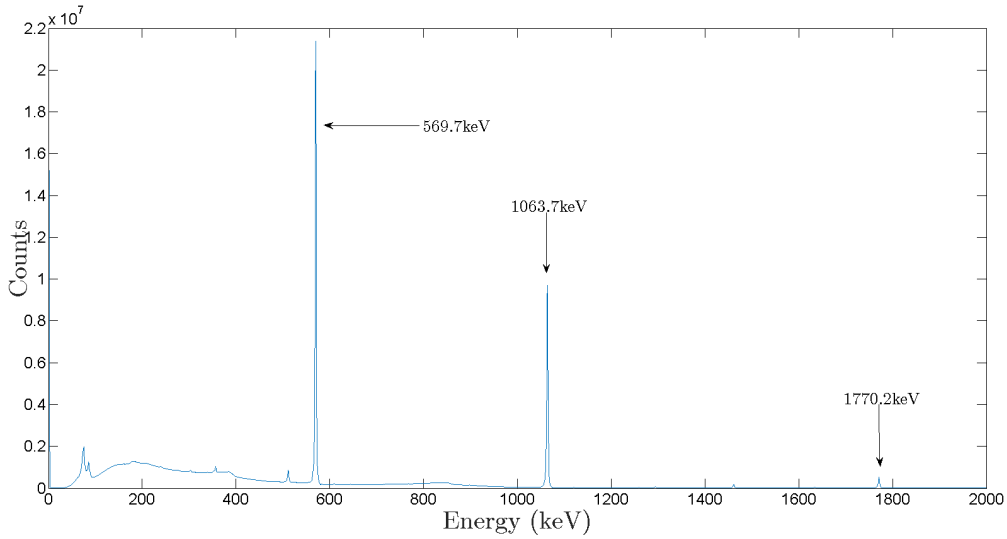

Figure 23: Bi-207 energy spectrum measured with the MINIBALL. The γ-ray energies from table 1 are labelled in the spectrum.

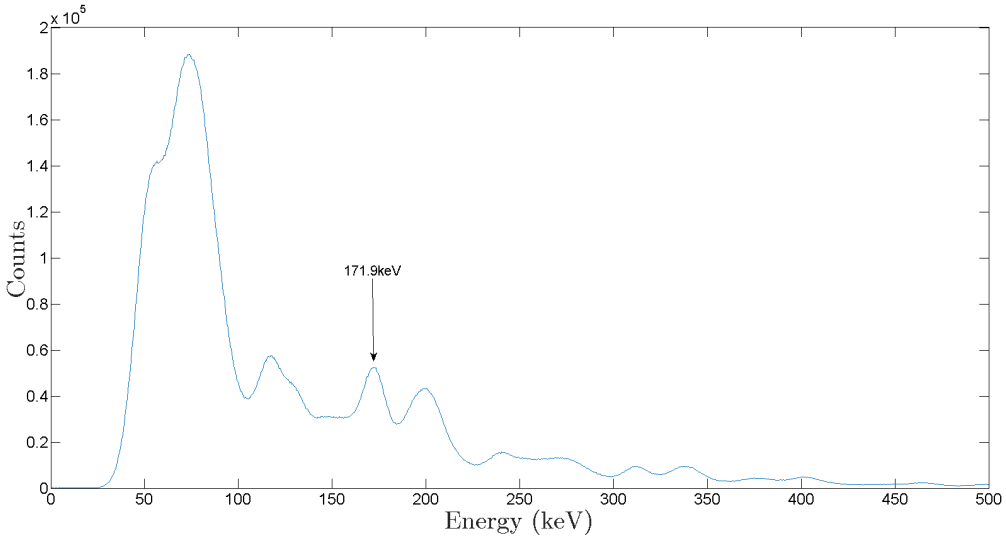

Figure 24: Hg-191 electron energy spectrum measured with SPEDE. Labelled peak contains different transitions, which are listed in table 6.

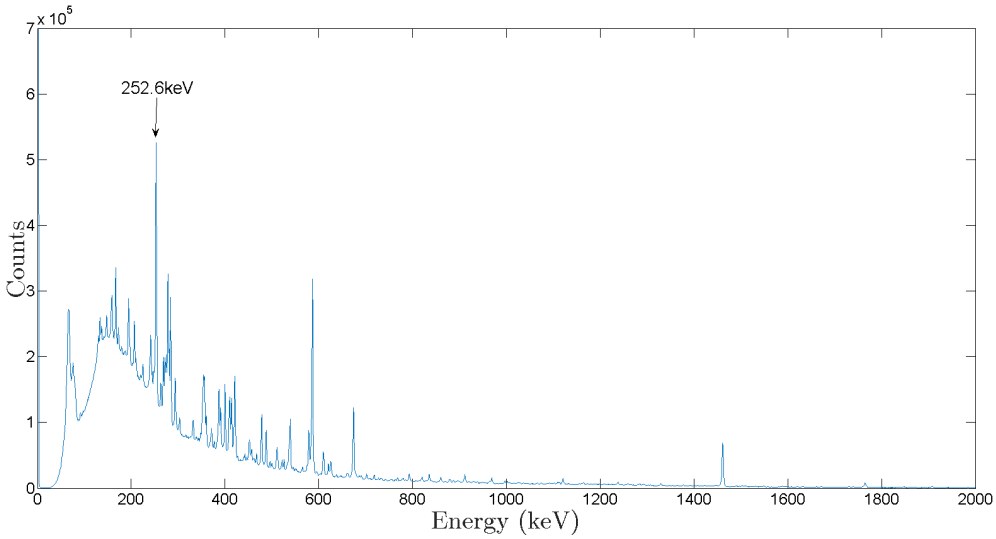

Figure 25: Hg-191 γ-ray energy spectrum measured with MINIBALL. The transition used in analysis has been labelled with its energy.

The resolution of SPEDE made precise measurements challenging, especially in cases such as Hg-191 where many transitions are present (see figure 25). This results in overlapping electron energies and peaks with components from different transitions (see figure 24). Solution for this problem is discussed in section 5.4.

5.2 Detection efficiency

Defining the detection efficiency of SPEDE and MINIBALL in the MINIBALL+SPEDE setup was done by combining the simulated efficiency curves, measured results for Bi-207 and known transition intensities (see table 1). The activity of the Bi-207 source was unknown so measuring the absolute efficiency was difficult. In this work, it is assumed that simulations well reproduce the shape of efficiency curve for the MINIBALL and SPEDE efficiency. The simulated efficiency has been found matching the measured one in previous measurements with SPEDE [39].

In determination of the measured efficiency of SPEDE and MINIBALL, the number of observed K-conversion electrons for the $5/2^- \rightarrow 1/2^-$ transition at energy 482keV were normalised to correspond with the simulated efficiency of SPEDE. The other measurement points are normalised accordingly. To obtain detection efficiency of MINIBALL, the simulated efficiency curve of MINIBALL was normalised to the measured efficiency of γ-rays obtained for the $5/2^- \rightarrow 1/2^-$ transition at energy 570keV.

The number of detected electrons N_{e^-E} and γ-rays $N_{\gamma\text{-}E}$ were determined by making a Gaussian fit on peaks labelled in figures 22 and 23. Fit results are listed in table 2. The uncertainty for the number of measured particles is assumed to be purely statistical

$$\Delta_{N_{i\text{-}E}} = \sqrt{C}, \tag{22}$$

where C is counts in the area of the Gaussian fit.

The efficiency is defined as

$$\epsilon_i(E) = \frac{N_{i\text{-}E}}{N_{s\text{-}E}}, \tag{23}$$

where i is either γ (γ-ray) or e^- (electron), E is energy, $N_{i\text{-}E}$ is the number of detected γ-rays or electrons at energy E and $N_{s\text{-}E}$ is the number of emitted γ-rays or electrons from source at energy E [23]. The detection efficiency of the SPEDE spectrometer was assumed to correspond simulated efficiency of SPEDE (see figure 20)

$$\epsilon_{e^-}(E) = \epsilon_{e^-sim}(E), \tag{24}$$

where $\epsilon_{e^-sim}(E)$ is simulated efficiency of electrons.

Measured data points were normalised using the K-conversion electrons for the $5/2^- \rightarrow 1/2^-$ transition at 482keV. The normalisation constant can be determined using known intensities and measured counts as follows

$$\mu = \frac{\epsilon_{e^-}(482) I_{e^-482}}{N_{e^-482}} = \frac{5.21\% \cdot 1.56\%}{1.4455 \cdot 10^6} = 5.63 \cdot 10^{-10}, \tag{25}$$

where I_{e^-482} is intensity of electrons at energy 482keV. The uncertainty of μ is calculated using the propagation of uncertainty

$$\begin{aligned} \Delta_\mu &= \sqrt{\left(\frac{\partial \mu}{\partial \epsilon_{e^-}(482)} \Delta_{\epsilon_{e^-}(482)}\right)^2 + \left(\frac{\partial \mu}{\partial I_{e^-482}} \Delta_{I_{e^-482}}\right)^2 + \left(\frac{\partial \mu}{\partial N_{e^-482}} \Delta_{N_{e^-482}}\right)^2} \\ &= \sqrt{\left(\frac{I_{e^-482}}{N_{e^-482}} \Delta_{\epsilon_{e^-}(482)}\right)^2 + \left(\frac{\epsilon_{e^-}(482)}{N_{e^-482}} \Delta_{I_{e^-482}}\right)^2 + \left(\frac{I_{e^-482}\epsilon_{e^-}(482)}{N^2_{e^-482}} \Delta_{N_{e^-482}}\right)^2} \\ &= 0.32 \times 10^{-11}. \end{aligned} \tag{26}$$

Measured efficiencies for the other data points of electrons are calculated employing the normalisation constant μ the following way

$$\epsilon_{e^-meas}(E) = \mu \frac{N_{e^-E}}{I_{e^-E}}. \tag{27}$$

The uncertainties of measured efficiencies $\epsilon_{e^-meas}(E)$ are obtained through the propagation of uncertainty. The values of N_{e^-E} and I_{e^-E} can be found in table 2. Measured efficiency and corresponding detection efficiency with uncertainties are listed in table 3 and plotted in figure 26.

Table 2: Energy, intensity [36] and number of counts obtained for transitions of interest in Bi-207 in the present work. Intensities are normalised to 100 decays.

SPEDE			
Transition	Energy (keV)	$I_{e^-E} \pm \Delta I_{e^-E}$ (%)	$(N_{e^-E} \pm \Delta_{N_{e^-E}}) \times 10^3$
$5/2^- \rightarrow 1/2^-$	481.7	1.56 ± 0.03	1445.5 ± 1.3
$5/2^- \rightarrow 1/2^-$	554.4	0.47 ± 0.02	413.3 ± 0.7
$13/2^+ \rightarrow 5/2^-$	975.7	7.17 ± 0.17	663.7 ± 0.9
$13/2^+ \rightarrow 5/2^-$	1048.1	1.91 ± 0.06	170.0 ± 0.5
MINIBALL			
Transition	Energy (keV)	$I_{\gamma E} \pm \Delta I_{\gamma E}$ (%)	$(N_{\gamma E} \pm \Delta_{N_{\gamma E}}) \times 10^4$
$5/2^- \rightarrow 1/2^-$	569.7	97.75 ± 0.39	5891.8 ± 0.8
$13/2^+ \rightarrow 5/2^-$	1063.6	74.09 ± 0.25	3221.5 ± 0.6
$7/2^- \rightarrow 5/2^-$	1770.2	6.87 ± 0.03	217.3 ± 0.1

One can calculate the measured efficiency of γ-rays for the $5/2^- \rightarrow 1/2^-$ using the definition of efficiency (see equation (23)) and the measured efficiency of electrons for the $5/2^- \rightarrow 1/2^-$ transition at energy 482keV

$$\begin{aligned} \epsilon_{\gamma\text{-}meas}(570) &= \frac{N_{\gamma\text{-}570}}{I_{\gamma\text{-}570} N_{tot}} = \frac{N_{\gamma\text{-}570} I_{e^-\text{-}482} \epsilon_{e^-}(482)}{I_{\gamma\text{-}570} N_{e^-\text{-}482}} \\ &= \frac{N_{\gamma\text{-}570} \mu \cancel{I_{e^-\text{-}482}} \cancel{N_{e^-\text{-}482}}}{I_{\gamma\text{-}570} \cancel{N_{e^-\text{-}482}} \cancel{I_{e^-\text{-}482}}} = \mu \frac{N_{\gamma\text{-}570}}{I_{\gamma\text{-}570}} = 3.39\%, \end{aligned} \tag{28}$$

where $N_{tot} = \frac{N_{e^-\text{-}482}}{I_{e^-\text{-}482} \epsilon_{e^-\text{-}482}}$ is the total number of emitted γ-rays and electrons and $N_{\gamma\text{-}570}$ and $I_{\gamma\text{-}570}$ can be found in table 2. Measured efficiency can therefore be written as

$$\epsilon_{\gamma\text{-}meas}(E) = \mu \frac{N_{\gamma\text{-}E}}{I_{\gamma\text{-}E}}. \tag{29}$$

The simulated γ-ray efficiency overestimated the measured γ-ray efficiency in the present work. This can be caused by the differences between experimental setup at measurement and simulation, for example thicknesses of materials and the distance between source and the γ-ray detectors, etc. Instead of modifying and optimising simulations to match experimental results, measures γ-ray yields were corrected using a normalisation constant as follows

$$\rho = \frac{\epsilon_{\gamma\text{-}meas}(570)}{\epsilon_{\gamma\text{-}sim}(570)} = \frac{3.39\%}{4.98\%} = 0.68. \tag{30}$$

Finally, the γ-ray detection efficiency can be calculated as follows

$$\epsilon_\gamma(E) = \rho \epsilon_{\gamma\text{-}sim}(E). \tag{31}$$

The $\epsilon_\gamma(E)$ values are plotted in figure 26. The detection efficiencies that are corresponding to measured efficiencies, are tabulated in table 3.

Table 3: Comparison of measured and detection efficiencies which are obtained for SPEDE and MINIBALL in the present work.

SPEDE		
Energy (keV)	$\epsilon_{e^-meas}(E) \pm \Delta_{\epsilon_{e^-meas}(E)}$ (%)	$\epsilon_{e^-}(E) \pm \Delta_{\epsilon_{e^-}(E)}$ (%)
481.7*	5.21 ± 0.32	5.21 ± 0.26
554.4	4.96 ± 0.31	5.07 ± 0.26
975.7	0.52 ± 0.04	2.30 ± 0.12
1048.1	0.50 ± 0.04	1.84 ± 0.10
MINIBALL		
Energy (keV)	$\epsilon_{\gamma-meas}(E) \pm \Delta_{\epsilon_{\gamma-meas}(E)}$ (%)	$\epsilon_{\gamma}(E) \pm \Delta_{\epsilon_{\gamma}(E)}$ (%)
569.7*	3.39 ± 0.20	3.39 ± 0.17
1063.6	2.45 ± 0.14	2.42 ± 0.12
1770.2	1.78 ± 0.11	1.79 ± 0.08

*Used in normalisation

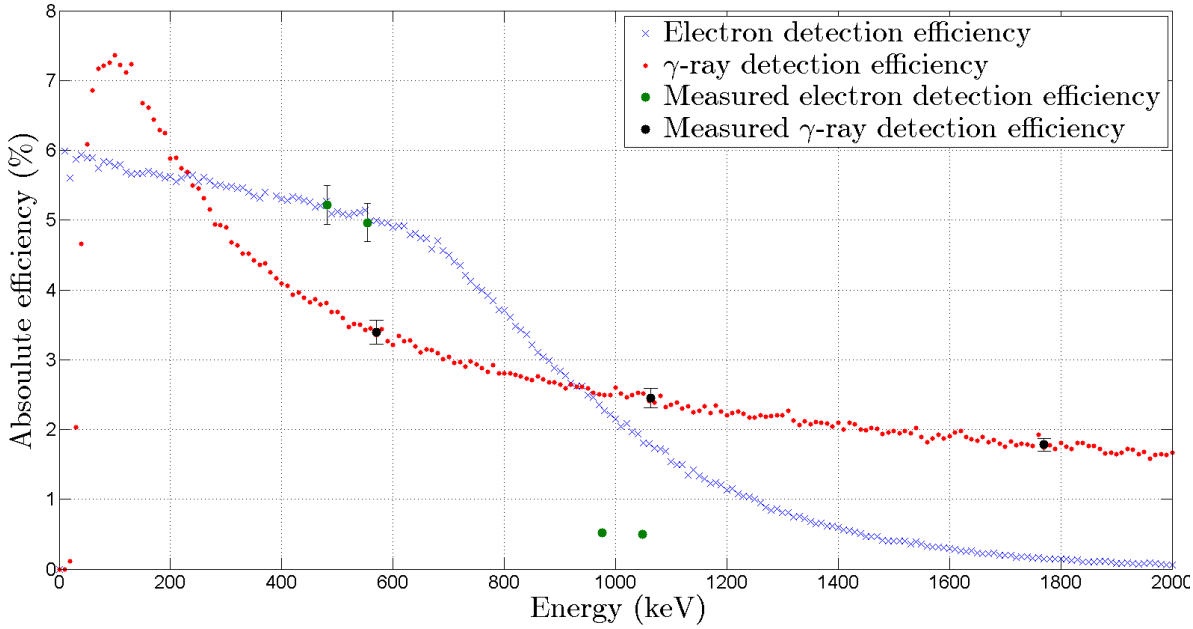

Figure 26: Detection and measured efficiencies of MINIBALL and SPEDE are obtained in the present work using Bi-207 source and simulations.

The figure 26 and table 3 shows also that the detection and measured efficiencies of SPEDE have discrepancies at higher energies ($\sim$ 900keV and above). The reason can be that electronics are cutting high amplitude signals off. The detection efficiency and measured γ-ray efficiency seem to behave similarly. The results on efficiency are discussed in more details in section 6. The detection efficiencies of SPEDE and MINIBALL are used in subsections 5.3 and 5.4.

5.3 $\alpha_{K/L}$-ratio of transitions following the decay of Bi-207

The $\alpha_{K/L}$-ratio was determined for the transitions following the decay of Bi-207 by using the measured number of counts in corresponding electron peaks (see table 2) and the efficiency of electrons (see figure 26). The equation for $\alpha_{K/L}$-ration can be written as

$$\alpha_{K/L} = \frac{\epsilon_L(E)N_K}{\epsilon_K(E)N_L}, \tag{32}$$

where N_K is the number of measured electrons of K-shell, N_L is the number of measured electrons of L-shell, $\epsilon_L(E)$ is efficiency for the L-shell electrons and $\epsilon_K(E)$ is efficiency for the K-shell electrons. The $\alpha_{K/L}$ values obtained in the present work, from literature [36] and calculated using BrIccFO [18] for the $5/2^- \rightarrow 1/2^-$ and $13/2^+ \rightarrow 5/2^-$ transitions in Bi-207 can be found in table 4.

Table 4: $\alpha_{K/L}$ ratios obtained for transitions in Bi-207 compared with literature [36] and values calculated with BrICC [18].

Transition	This work	Literature measurements	Theoretical prediction
$5/2^- \rightarrow 1/2^-$	3.29 ± 0.06	3.33 ± 0.05	3.61 ± 0.08
$13/2^+ \rightarrow 5/2^-$	3.11 ± 0.05	3.75 ± 0.06	3.96 ± 0.09

The values obtained with SPEDE confirm the values from previous measurements for the $5/2^- \rightarrow 3/2^-$ transition [36]. The deviation of the measured $\alpha_{K/L}$ value for the $13/2^+ \rightarrow 5/2^-$ transition from literature values can be explained by SPEDE signal readout issues at higher energies. The theoretically calculated values differ from the literature and this work values.

5.4 Partial K-electron ICC-value for the $5/2^+ \rightarrow 3/2^+$ transition in Au-191

SPEDE was used to determine the partial ICC α_{Kmeas} (see equation (17)) for the $5/2^+ \rightarrow 3/2^+$ transition at 253keV in Au-191 that is the decay product of Hg-191 [9]. The peaks of interest are labelled in Hg-191 spectra (see figures 24 and 25). The number of detected electrons and γ-rays are listed in table 5. A Gaussian fit was performed for a peak ranging between 160-185keV in Hg-191 electron spectrum. Conversion electrons of Au-191 and Pt-191, between 160-185keV energy range, was taken to account, according to [9]. The Ir-191 has no conversion electrons in the 160-185keV energy range [40].

The partial ICC for the K-conversion electron of the $5/2^+ \rightarrow 3/2^+$ transition in Au-191 can be extracted as

$$\alpha_{Kmeas} = \frac{\epsilon_\gamma(253)N_{e^-corr\text{-}172}}{\epsilon_{e^-}(172)N_{\gamma\text{-}253}}, \tag{33}$$

where $\epsilon_\gamma(253)$ and $\epsilon_{e^-}(172)$ are efficiencies of γ-ray and electron, $N_{\gamma 253}$ is detected number of γ-rays and $N_{e^-corr\text{-}172}$ is the number of K-conversion electron of the $5/2^+ \rightarrow 3/2^+$ transition. To determine partial ICC α_{Kmeas}, one needs to calculate the corrected number of electrons $N_{e^-corr\text{-}172}$.

Table 5: Detected number of electrons and γ-rays for the $5/2^+ \rightarrow 3/2^+$ transition in Au-191. Efficiencies are also included in table.

SPEDE		
Energy (keV)	$\epsilon_{e^-}(172) \pm \Delta_{\epsilon_{e^-}(172)}(\%)$	$N_{e^-172} \pm \Delta_{N_{e^-172}}$
171.9	5.66 ± 29	319433 ± 566
MINIBALL		
Energy (keV)	$\epsilon_\gamma(253) \pm \Delta_{\epsilon_\gamma(253)}(\%)$	$N_{\gamma\text{-}253} \pm \Delta_{N_{\gamma\text{-}253}}$
252.6	5.41 ± 0.27	789840 ± 889

The number of electrons N_{e^-172}, in 160-185keV energy range, can be defined by sum of Au-191 and Pt-191 intensities of conversion electrons that are shown in table 6. The number of electrons was obtained as follows

$$\begin{aligned} N_{e^-172} &= \sum_j (N_{j\text{-}Au\text{-}E}) + \sum_k (N_{k\text{-}Pt\text{-}E}) \\ &= \sum_j \left(\frac{I_{j\text{-}E}}{I_{e^-172}} \right) N_{e^-corr\text{-}172} + \sum_k \sigma \left(\frac{I_{k\text{-}E}}{I_{e^-172}} \right) N_{e^-corr\text{-}172}, \end{aligned} \tag{34}$$

where $N_{j\text{-}Au\text{-}E}$ is the number of electron conversion electron for transition j of Au-191, $I_{j\text{-}E}$ is the intensity for transition j of Au-191, $N_{k\text{-}Pt\text{-}E}$ is the number of conversion electrons for transition k of Pt-191, $I_{k\text{-}E}$ is the intensity for transition k of Pt-191, $N_{e^-corr\text{-}172}$ is the corrected number of electrons at energy 172keV and σ is ratio between Au-191 and Hg-191 decays.

Table 6: Conversion electrons following the decay of Hg-191 between 160-185keV energy range. Table includes energy of electron, intensity and uncertainty of intensity [9].

Au-191		
Energy (keV)	$I_{j\text{-}E}$ (%)	$\Delta_{Ij\text{-}E}$ (%)
161.7	1.3	0.1
171.9	16.0	9.0
182.1	0.4	0.2
Pt-191		
Energy	$I_{k\text{-}E}$ (%)	$\Delta_{Ik\text{-}E}$ (%)
163.2	0.164	0.021
165.8	0.04	0.005
166.0	0.3	0.04
166.5	0.007	0.0009
169.1	0.097	0.019
175.6	0.21	0.03
178.9	0.037	0.006
180.2	0.34	0.04
184.7	0.116	0.014

The ratio between Hg-191 and Au-191 decays σ was determined from the number of

measured γ-rays as follows

$$\sigma = \frac{\epsilon_\gamma(611) I_{\gamma\text{-}611} N_{\gamma\text{-}478}}{\epsilon_\gamma(478) I_{\gamma\text{-}478} N_{\gamma\text{-}611}} = 2.63 \pm 1.61, \tag{35}$$

where $N_{\gamma\text{-}611}$ is the number of observed γ-rays at energy 611keV in the decay of Hg-191, $I_{\gamma\text{-}611}$ is the intensity of the 611keV transition in the decay of Hg-191 [9], $N_{\gamma\text{-}478}$ is the number of observed γ-rays at energy 478keV in the decay of Au-191, $I_{\gamma\text{-}478}$ is the intensity of the 478keV transition in the decay of Au-191 [9] and $\epsilon_\gamma(611)$ and $\epsilon_\gamma(478)$ are the γ-ray detection efficiencies at energy 611keV and 478keV. Numbers to calculate the decay ratio σ are listed in table 7.

Table 7: Decay products of Hg-191 and Au-191. Table contains energy, simulated efficiencies, intensities and measured number of particles. Intensities are taken from [9].

Decay product	Energy (keV)	$I_{\gamma\text{-}E} \pm \Delta_{I_{\gamma\text{-}E}}(\%)$	$\epsilon_\gamma(E) \pm \Delta_{\epsilon_\gamma(E)}(\%)$	$(N_{\gamma\text{-}E} \pm \Delta_{N_{\gamma\text{-}E}})$
^{191}Au	610.6	5 ± 3	3.73 ± 0.19	112300 ± 336
^{191}Pt	478.0	3.5 ± 0.4	3.30 ± 0.17	183041 ± 428

The corrected number of conversion electrons for the $5/2^+ \rightarrow 3/2^+$ transition can be obtained by using equation (34), value of σ (35), the measured number of electrons in table 5 and intensities in table 6 as follows

$$\begin{aligned} N_{e^\text{-}corr\text{-}172} &= \left(\sum_j \left(\frac{I_{j\text{-}E}}{I_{e^\text{-}172}} \right) + \sigma \sum_k \left(\frac{I_{k\text{-}E}}{I_{e^\text{-}172}} \right) \right)^{-1} N_{e^\text{-}\text{-}172} \\ &= 241990 \pm 105967. \end{aligned} \tag{36}$$

By using the result of the corrected number of conversion electron (36) and the values of table 5, the result of partial ICC equation (33) can be calculated

$$\alpha_{K meas} = \frac{\epsilon_\gamma(253) N_{e^\text{-}corr\text{-}172}}{\epsilon_e(172) N_{\gamma\text{-}253}} = 0.30 \pm 0.13. \tag{37}$$

The result for the theoretical value of ICC obtained with BrIccFO [18] is

$$\alpha_{K theor} = 0.28 \pm 0.01. \tag{38}$$

The $5/2^+ \rightarrow 3/2^+$ transition is a mixture of E2 and M1 transitions with mixing ratio $\delta = 0.9$ [41]. In theoretical calculation, mixing ratio $\delta = 0.9$ was used. The $\alpha_{K meas} = 0.30 \pm 0.13$ is in good agreement with theoretical prediction for $\alpha_{K theor} = 0.28 \pm 0.01$. This emphasizes the importance of good understanding of measured results. Moreover, it highlights the importance of good spectrometer performance that would help making deconvolution of peaks easier.

6 Conclusion

In the present work, the functionality of SPEDE in MINIBALL and its electronics was tested in the final experimental location. Well-known Bi-207 and custom made Hg-191 sources were used to make experiment with SPEDE. The results show that SPEDE is a potential tool to detect conversion electrons and can provide better understanding of structure of the atomic nucleus. Also, results show that one should improve the resolution before any Coulomb excitation experiments.

The electronics used in the present work did not cope well with the SPEDE signal, resulting in poor electron energy resolution, which in turn made the interpretation of results challenging. When the GO-unit signal was tested with Lyrtech cards, much better resolution was obtained. However, these electronics will be upgraded soon and the SPEDE experimental campaign will employ new digitisers.

In this thesis, the detection efficiency curves 26 of SPEDE and MINIBALL was obtained by combining simulation and experimental results. The discrepancies between detection and measured efficiencies can also be explained by the used electronics. This will be further assessed with different electronics solutions, e.g. with existing analogue electronics and using the new MINIBALL electronics after upgrade.

The $\alpha_{K/L}$ ratio obtained for the $5/2^- \rightarrow 1/2^-$ transition in Bi-207 was consisted with earlier results [36]. The discrepancy between the $\alpha_{K/L}$ value obtained for the $13/2^+ \rightarrow 5/2^-$ transition in Bi-207 with SPEDE and literature can again be explained by the used electronics.

The α_K was determined for the $5/2^+ \rightarrow 3/2^+$ transition in Au-191. A careful deconvolution of the peak stemming for the $5/2^+ \rightarrow 3/2^+$ transition in the electron energy spectrum was needed for reliable analysis. However, the value obtained confirms, within uncertainties, the theoretical value.

It has been shown that SPEDE can be used in MINIBALL to detect internal conversion electrons. SPEDE will bring new technique to the MINIBALL experimental setup to study properties of atomic nucleus. It will allow for direct observation of conversion electrons in-beam and will be essential in cases where atomic nuclei posses the $0^+ \rightarrow 0^+$ transition. These new possibilities make SPEDE a great addition to the MINIBALL experimental setup.

References

[1] R. Parry. Empedocles. `https://stanford.library.sydney.edu.au/archives/fall2008/entries/empedocles/`.

[2] K. S. Krane. *Introdroductory nuclear physics.* John Willey & Sons Ltd., 1988.

[3] H. E. Roscoe and A Harden. *A New View of the Origin of Dalton's Atomic Theory.* MacMillan and Co., 1896.

[4] E. Rutherford. Lxxix. the scattering of and particles by matter and the structure of the atom. *Philosophical Magazine Series 6*, 21(125):669–688, 1911.

[5] J. Lilley. *Nuclear physics priciples and application.* John Willey & Sons Ltd., 2001.

[6] K. L. G. Heyde. *Basic Ideas and Concepts in Nuclear Physics : an Introductory Approach.* Fundamental and applied nuclear physics series. Institute of Physics Publishing, Bristol, 3rd ed edition, 2004.

[7] E. Gapon and D. Iwanenko. Zur bestimmung der isotopenzahl. *Naturwissenschaften*, 20(43):792–793, 1932.

[8] J. Suhonen. *From Nucleons to Nucleus; Consepts of micrscopic nuclear theory.* Springer, 2007.

[9] Brookhaven National Laboratory National Nuclear Data Center. Nudat (nuclear structure and decay data). `http://www.nndc.bnl.gov/nudat2/`, March 18, 2008 2008.

[10] R. F. Casten. *Nuclear Structure from a Simple Perspective.* Oxford University Press (US), 1990.

[11] K. Alder, A. Bohr, T. Huus, B. Mottelson, and A. Winther. Study of nuclear structure by electromagnetic excitation with accelerated ions. *Rev. Mod. Phys.*, 28:432–542, Oct 1956.

[12] A. Bohr and B. R. Mottelson. *Nuclear Structure.* Number v. 2 in Nuclear Structure. World Scientific, 1998.

[13] J. Kantele. *Handbook of nuclear Spectrometry.* Academic Press, 1995.

[14] T. Kibédi and R. H. Spear. Electric monopole transitions between 0+ states for nuclei throughout the periodic table. *AIP Conference Proceedings*, 769(1):442–445, 2005.

[15] J. L. Wood, E. F. Zganjar, C. De Coster, and K. Heyde. Electric monopole transitions from low energy excitations in nuclei. *Nuclear Physics A*, 651(4):323 – 368, 1999.

[16] H. R. Hulme. The internal conversion coefficient for radium c. *Proceedings of the Royal Society of London A: Mathematical, Physical and Engineering Sciences*, 138(836):643–664, 1932.

[17] T. Kibédi, T. W. Burrows, M. B. Trzhaskovskaya, P. M. Davidson, and C. W. Nestor Jr. Evaluation of theoretical conversion coefficients using BrIcc. *Nuclear Instruments and Methods in Physics Research Section A: Accelerators, Spectrometers, Detectors and Associated Equipment*, 589(2):202 – 229, 2008.

[18] BrIcc v2.3s conversion coefficient calculator. `http://bricc.anu.edu.au/`.

[19] D. Cline. Nuclear shapes studied by coulomb excitation. *Annual Review of Nuclear and Particle Science*, 36(1):683–716, 1986.

[20] A. Görgen. Shapes and collectivity of exotic nuclei via low-energy coulomb excitation. *Journal of Physics G: Nuclear and Particle Physics*, 37(10):103101, 2010.

[21] J. Pakarinen, D. Voulot, F. Wenander, J. Simpson, Th. Kröll, T. Davinson, E. Clément, T. Grahn, P. T. Greenlees, and P. Jones. In-beam electron spectroscopy at HIE-ISOLDE. *Default journal*, 2010.

[22] R. Julin. Gamma-ray and conversion-electron spectroscopy of exotic heavy nuclei, lect. notes. 2004.

[23] G. F. Knoll. *Radiation Detection and Measurement*. John Wiley & Sons, 2010.

[24] A. Herlet. The isolde facility. *Nuclear Physics News*, 20(4), 2010.

[25] P. Van Duppen and K. Riisager. Physics with REX-ISOLDE: from experiment to facility. *Journal of Physics G: Nuclear and Particle Physics*, 38(2):024005, 2011.

[26] Isolde web page about REX-Isolde. `http://rex-isolde.web.cern.ch/`.

[27] A. Herlert and Y. Kadi. The HIE-ISOLDE project. *Journal of Physics: Conference Series*, 312(5):052010, 2011.

[28] N. Warr, J. Van de Walle, and et al. The Miniball spectrometer. *The European Physical Journal A*, 49(3):1–32, 2013.

[29] J. Eberth, G. Pascovici, H.G. Thomas, N. Warr, D. Weisshaar, D. Habs, P. Reiter, P. Thirolf, D. Schwalm, C. Gund, H. Scheit, M. Lauer, P. Van Duppen, S. Franchoo, M. Huyse, R.M. Lieder, W. Gast, J. Gerl, and K.P. Lieb. MINIBALL a ge detector array for radioactive ion beam facilities. *Progress in Particle and Nuclear Physics*, 46(1):389 – 398, 2001.

[30] Isolde webpage about MINIBALL. `http://isolde.web.cern.ch/experiments/miniball`.

[31] The miniball double-sided silicon strip detector (CD). `http://www.ikp.uni-koeln.de/~warr/doc/cd.pdf`.

[32] P. Papadakis. The SPEDE spectrometer: Combined in-beam γ -ray and conversion electron spectroscopy with radioactive ion beams. *JPS*, Proc.6:36–48, 2015.

[33] J. Konki, P. Papadakis, and J. Pakarinen et al. Combined in-beam gamma-ray and conversion electron spectroscopy with radioactive ion beams. *EPJ Web of Conferences*, 63:01019, 2013.

[34] P. Papadakis. Results from the first tests with the SPEDE spectrometer. *ISOLDE Workshop and Users Meeting*, 2014.

[35] Charge sensitive preamplifier A259F/NF. `http://amptek.com/products/a250f-and-a250fnf-high-density-charge-sensitive-preamplifiers/#2`.

[36] W.H. Trzaska. Recommended data on selected gamma-ray and conversion-electron calibration sources. *Nuclear Instruments and Methods in Physics Research Section A: Accelerators, Spectrometers, Detectors and Associated Equipment*, 297(1):223 – 229, 1990.

[37] Root web page. `https://root.cern.ch`.

[38] S. Agostinelli et al. Geant4—a simulation toolkit. *Nuclear Instruments and Methods in Physics Research Section A: Accelerators, Spectrometers, Detectors and Associated Equipment*, 506(3):250 – 303, 2003.

[39] D. M. Cox. Private communications.

[40] A. Bäcklin, G. Hedin, and S.G. Malmskog. Levels in 191ir. *Nuclear Physics A*, 169(1):122 – 130, 1971.

[41] V. R. Vanin, N. L. Maidana, R. M. Castro, E. Achterberg, O. A. Capurro, and G. V. Martí. Nuclear data sheets for a = 191. *Nuclear Data Sheets*, 108(11):2393 – 2588, 2007.